NTNU

Norwegian University of
Science and Technology

Finite Element Modeling of Piezoelectric Ultrasonic Transducers

Morten Wollert Nygren

Master of Science in Electronics
Submission date: January 2011
Supervisor: Trond Ytterdal, IET
Co-supervisor: Tonni Franke Johansen, ISB

Norwegian University of Science and Technology
Department of Electronics and Telecommunications

Problem Description

A series of piezoelectric ultrasonic transducer with increasing complexity is to be modeled in the finite element analysis program COMSOL Multiphysics, and compared to a one-dimentional model as long as such a comparison is reasonable. The final model will be a thick film piezoelectric layer deposited on a spherical cap.

Assignment given: 26. August 2010
Supervisor: Trond Ytterdal, IET

Abstract

The optimization of piezoelectric ultrasonic transducers has tradisionally been done through trial and error, somewhat guided by one-dimentional simulations. This can often be a very time-consuming and expensive process, hence a more extensive simulation method is desired.

A series of finite element models of piezoelectric ultrasonic transducer has been made in COMSOL Multiphysics. The initial models were designed to emulate the conditions assumed in a one-dimentional transducer model, and their validity could thus be confirmed by said model. Later models did not emulate these conditions, and a lossless model of a spherical disc with backing and a single matching layer was successfully implemented. Attemps had been made to include mechanical loss in the initial models, but was only partially achieved. All loss was thus excluded from later models. A final model with a piezoelectric layer poled in the radial direction was not successfully designed, as the varying poling direction proved to be difficult to implement.

I

Preface

This thesis, and the work it presents, is the culmination of my masters degree at the Department of Electronics and Telecommunication of the Norwegian University of Science and Technology (NTNU). I would like to thank my supervisor Tonni Franke Johansen for his patience, and his guidance it the fields of acoustics, piezoelectrics and finite element modelling. I am also very grateful to everyone else who have given me input and feedback over the last couple of months.

Contents

List of Figures

VIII

List of Tables

IX

X

Chapter 1

Introduction

Ultrasound is the collective name of all soundwaves above the range of human hearing, i.e. above 20 kHz. Such waves were in the thirties the foundation of the invention of SONAR, which operates at frequencies from 20kHz to 100kHz. The variety of applications for ultrasound increased significantly with the discovery of piezoelectric ceramics[2], allowing for frequencies in the range of MHz. These high frequencies gave rise to non-intrusive analysis of solid material, such as in welding seams. It was soon realized that the non-intrusive nature of ultrasound would make it an exellent tool in medical diagnostic, and successful studies of the human body was conducted in the U.S.[27], Japan[24] and Sweden[7] in the late forties and early fifthies.

The development of ultrasound in medicine over the last sixty years has been phenomenal, giving rise to, for example, real time three-dimentional ultrasound[21]. A large part of this development was made possible by the advances in computer technology, allowing for processing of vast amounts of data in a short period of time. However, the development of new ultrasonic transducers is also of great importance, as the signal processing is ultimately limited by the quality of the input data. The method of designing new transducer has tradisionally been based on trial and error, supplemented by one-dimentional simulations. This can however be very expensive and time-comsuming, as several transducers may have to be constructed in order to optimize a design. A computer simulation of complete transducer designs is therefore desired, and for this is the finite element method a very good candidate.

The basis of the finite element method was developed seperately by mathematicians, physicists and engineers, as a way of decomposing complex problems into simple well known parts. The initial use of the method in engineering was to replace plates with simple struts[9], but it has later developed into covering a wide variety of applications, including acoustics[11] and

piezoelectricity[13].

The work in this thesis will employ these two branches of physics in a series of finite element models of ultrasonic piezoelectric transducers. The first models will be designed to emulate a one-dimentional problem, thus allowing their validity to be verified by known one-dimentional models. The final model will be of a transducer in the shape of a spherical cap, where the piezoelectric layer is a deposited thick film. For all simulations will two parameters be obtained, namely the inductance, Y, and the average velocity on the transducer surface relative to the applied voltage, Htt.

Chapter 2

Theory

2.1 Acoustic propagation

2.1.1 Stress and strain

An accoustic wave, ultrasonic or otherwise, is essentially a mechanical deformation propagating through a material, and can for this reason be described by the relation between stress and strain. Within a body subjected to external forces is a unit cube as seen in figure 2.1. Stress is, as seen in the
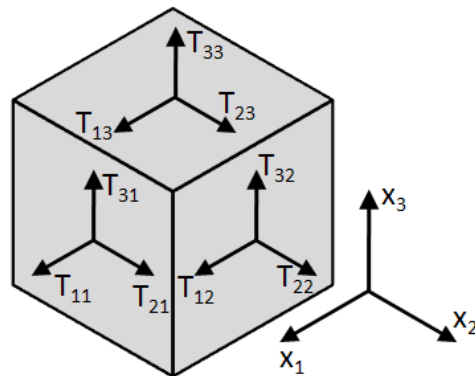
Figure 2.1: Directions of normal and shear stresses.

figure, defined as the force per unit area in direction i acting on the surface of the unit cube whose normal is direction j. The components where $i = j$ are the normal or longitudinal stresses, while those where $i \neq j$ are the shear stresses. The stresses acting on the three opposite faces that can not be seen in the figure of the cube are all of the same magnitude but opposite direction as those that are seen, consequently the net force acting on the cube is

zero. Furthermore, any stress component T_{ij} will be equal to Tji for $i \neq j$ to prevent the cube from rotating. The six independent stress components are often represented as a vector with the following index convention:

$$
\begin{array}{ll}
T_{11} = T_1 & T_{23} = T_{32} = T_4 \\
T_{22} = T_2 & T_{13} = T_{31} = T_5 \\
T_{33} = T_3 & T_{12} = T_{21} = T_6
\end{array}
$$

Strain is a quantification of the deformation of the unit cube. It is divided into normal strains, as seen in figure 2.2(a), and shear strain which is illustrated in 2.2(b). The index notation of the strains is similar to that of the stresses, with i indicating the direction of the deformation and j the suface which is deformed. All the strains are defined as follows:

$$
S_{ij} = \frac{1}{2} \frac{\partial \Psi_i}{\partial x_j} + \frac{\partial \Psi_j}{\partial x_i} \tag{2.1}
$$

Strains are also often represented as a vector, following the same index convention as the stresses.

(a) Normal or longitudinal strain   (b) Shear strain
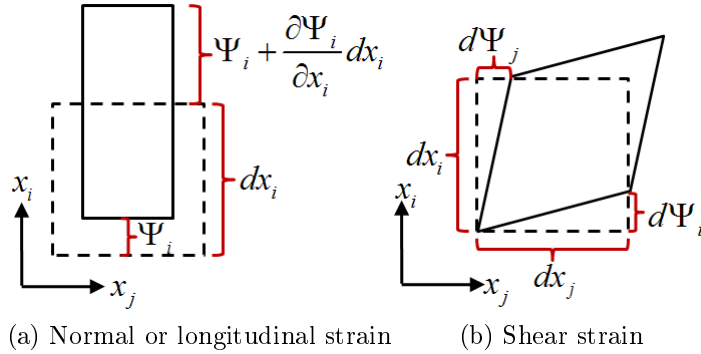
Figure 2.2: The definition of normal and shear strain

The relation between stress and strain in a material is linear, assuming that the strains are small and the material follows Hooke's law (i.e. is elastic). This relation for an arbitrary material will then be expressed by the generalized Hooke's law which is show in its matrix form in eq 2.2.

$$
\begin{bmatrix} T_1 \\ T_2 \\ T_3 \\ T_4 \\ T_5 \\ T_6 \end{bmatrix} = \begin{bmatrix} c_{11} & c_{12} & c_{13} & c_{14} & c_{15} & c_{16} \\ c_{21} & c_{22} & c_{23} & c_{24} & c_{25} & c_{26} \\ c_{31} & c_{32} & c_{33} & c_{34} & c_{35} & c_{36} \\ c_{41} & c_{42} & c_{43} & c_{44} & c_{45} & c_{46} \\ c_{51} & c_{52} & c_{53} & c_{54} & c_{55} & c_{56} \\ c_{61} & c_{62} & c_{63} & c_{64} & c_{65} & c_{66} \end{bmatrix} \begin{bmatrix} S_1 \\ S_2 \\ S_3 \\ S_4 \\ S_5 \\ S_6 \end{bmatrix} \tag{2.2}
$$

Where c is the (elastic) stiffness matrix of the material. However, the stiffness matrix can be simplified by considering the symmetries in a given material, such as in a isotropic material, where eq 2.2 will be modified as follows.

$$
\begin{bmatrix} T_1 \\ T_2 \\ T_3 \\ T_4 \\ T_5 \\ T_6 \end{bmatrix} = \begin{bmatrix} \lambda + 2\mu & \lambda & \lambda & 0 & 0 & 0 \\ \lambda & \lambda + 2\mu & \lambda & 0 & 0 & 0 \\ \lambda & \lambda & \lambda + 2\mu & 0 & 0 & 0 \\ 0 & 0 & 0 & 2\mu & 0 & 0 \\ 0 & 0 & 0 & 0 & 2\mu & 0 \\ 0 & 0 & 0 & 0 & 0 & 2\mu \end{bmatrix} \begin{bmatrix} S_1 \\ S_2 \\ S_3 \\ S_4 \\ S_5 \\ S_6 \end{bmatrix} \tag{2.3}
$$

Here is λ and μ the first and second Lamé-constants. This equation gives a complete description of the mechanical properties of a linear-elastic, lossless and isotropic material.

2.1.2   Wave equation

An expression for motion of the unit cube in fig 2.1 can be described by calculating the net force to which it is subjected. In other words, by applying Newton's second law. A situation where there is only motion in the 3-direction will then be expressed as follows:

$$
\frac{\partial T_3}{\partial x_3} + \frac{\partial T_4}{\partial x_2} + \frac{\partial T_5}{\partial x_1} = \rho \frac{\partial^2 \Psi_3}{\partial t^2} \tag{2.4}
$$

Where ρ is the mass density of the material, t is time and Ψ_3 is the displacement of the unit cube in the 3-direction. In a solid there can exist both longitudinal, or pressure, waves and transversal, or shear, waves. They differ in the direction of displacement relative to the propagation direction of the wave, as seen in figures 2.3 and 2.4. If a shear wave propagating in the 1-direction is causing the motion in eq 2.4, then S_5 will be the only non-zero strain component. Consequently will the only non-zero stress compont be T_5 and eq 2.4 can be reduced to:

$$
\frac{\partial T_5}{\partial x_1} = \rho \frac{\partial^2 \Psi_3}{\partial t^2} \tag{2.5}
$$

Furthermore can eqs 2.3 and 2.1 be used to express the stress as a displacement resulting in:

$$
\frac{\partial^2 \Psi_3}{\partial x_1^2} = \rho \frac{\partial^2 \Psi_3}{\partial t^2} \tag{2.6}
$$

This is recognized as the wave equation, which has a sinusodial solution:

$$
\Psi_3^{\mp}(x_3, t) = \Psi_{3,0} e^{j(\omega t \pm k x_3)} \tag{2.7}
$$

Where Ψ_3^- and Ψ_3^+ represent the positive- and negative-traveling wave, respectively, while $\omega = 2\pi f$ is the angular frequency and $k = \frac{\omega}{c}$ is the wavenumber. Eqs 2.6 and 2.7 will also show that the propagation speed of a shear wave is:

$$c_s = \sqrt{\frac{\mu}{\rho}} \tag{2.8}$$

It must be noted that a shear wave can only propagate in a solid, as $\mu = 0$ in both liquids and gases. This is however not the case for a pressure wave.
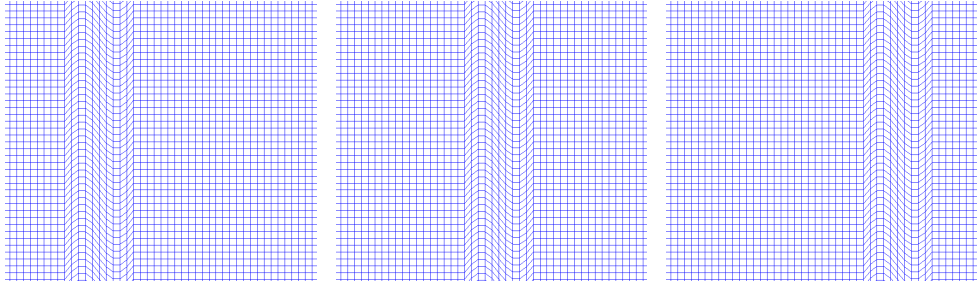
Figure 2.3: The propagation of a plane shear wave
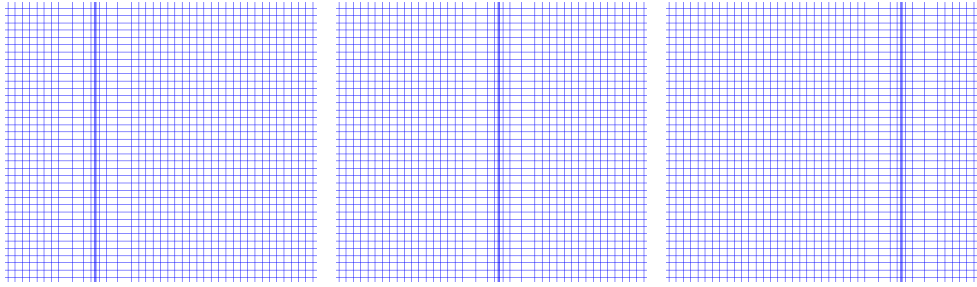
Figure 2.4: The propagation of a plane pressure/longitudinal wave

The propagation of a plane longitudinal wave will be without any shear strain, and normal strain only in the direction the wave is propagating, as seen in figure 2.4. This will cause eq 2.4 to be reduced to:

$$\frac{\partial T_3}{\partial x_3} = \rho \frac{\partial^2 \Psi_3}{\partial t^2} \tag{2.9}$$

The same assumption will, when applied to eq 2.3 show that the relation between T_3 and S_3 in this case becomes:

$$T_3 = (\lambda + 2\mu)S_3 = (\lambda + 2\mu)\frac{\partial \Psi_3}{\partial x_3} \tag{2.10}$$

6

Here the definition of strain is used to show the relation between stress and displacement. Eq 2.10 is then substituted into eq 2.9:

$$\frac{\partial^2 \Psi_3}{\partial x_3^2} = \frac{\rho}{\lambda + 2\mu} \frac{\partial^2 \Psi_3}{\partial t^2} \tag{2.11}$$

This is identified as the wave equation, with the sinusodial solution:

$$\Psi_3^{\mp}(x_3, t) = \Psi_{3,0} e^{j(\omega t \pm k x_3)} \tag{2.12}$$

Eqs 2.11 and 2.12 can, in a similar way as with the shear wave, show that the propagation speed of a longitudinal wave in a solid is:

$$c_l = \sqrt{\frac{\lambda + 2\mu}{\rho}} = \sqrt{\frac{M}{\rho}} \tag{2.13}$$

Where M is the p-wave, or longitudinal, modulus. But if the wave is propagating through a liquid or gas is $\mu = 0$ and eq 2.13 will be altered to:

$$c_l = \sqrt{\frac{\lambda}{\rho}} = \sqrt{\frac{B}{\rho}} \tag{2.14}$$

Where B is the bulk modulus of the material, representing is resistance to compression.

2.1.3 Acoustic Impedance

The displacement Ψ_3, as described in eq 2.12 can be differentiated with respect to time in order to obtain the rate of change in displacement, u_3, also known as the particle velocity:

$$u_3 = \frac{\partial \Psi_3}{\partial t} = j\omega \Psi_3 \tag{2.15}$$

When viewing the definition of stress in section 2.1.1 it is apparent that normal stress on a surface is equal to pressure in magnitude. It is however positive in the opposite direction, since a positive normal stress will cause tension, while a positive pressure will cause compression. Inserting this relation into eq 2.10 gives:

$$p = -(\lambda + 2\mu) \frac{\partial \Psi_3}{\partial x_3} \tag{2.16}$$

Φ_3 is given in eq 2.12 and can with eqs 2.13 and 2.15 be used to change eq 2.16 into:

$$p^{\pm} = \pm jk(\lambda + 2\mu)\Psi_3^{\pm} = \pm j\omega \rho c_l \Psi_3^{\pm} = \pm \rho c_l u_3^{\pm} \tag{2.17}$$

Rearranging this equation will give the characteristic acoustic impedance for a longitudinal wave:

$$Z_l^\pm = \frac{p^\pm}{u_3^\pm} = \pm\rho c_l \tag{2.18}$$

2.2 The piezoelectric effect

2.2.1 Mechanism

Certain materials will generate an electric charge when subjected to a mechanical stress, and change its dimentions when an electric field is applied across the material. These are known respectively as the direct and the inverse piezoelectric effect[4]. The effect is observed in a variety of materials, such as quartz, dry bone, polyvinylindene fluoride $(-(C_2H_2F_2)_n-)$ and lead zirconate titanate $(Pb[Zr_xTi_{1-x}]O_3, 0 < x < 1)$. The latter of these, also known by the abbreviation PZT, is a man-made ceramic with a perovskite structure, and one of the most commonly used piezoelectric ceramics today. It is also the piezoelectric material used in the simulations in this thesis.

The piezoelectric effect can only occur in anisotropic materials[1], which implies that a crystalline piezoelectric material must have a noncentrosymmetric structure. An example of this is the previously mentioned PZT where the positive Ti/Zr ion is positioned a bit off center in the lattice, causing a polarization in the same direction, as seen to the right in figure 2.5. An external mechanical strain will deform the lattice, thus move the Ti/Zr ion and change the magnitude of the polarization. While an applied electric field will move the Ti/Zr ion and as a consequence the lattice, and thus the material, will be deformed. However, an isotropic material can have a change in dimentions when an electric field is applied, but there will be no generated charge when the material is subjected to mechanical pressure. This is caused by a small nonlinear effect known as the electrostrictive effect, while the piezoelectric effect is linear[28]. Initially, the dipoles in PZT are polarized in random directions resulting little or no polarization of the material as a whole, and thus little or no piezoelectric effect. This problem can in some piezoelectric materials, PZT included, be addressed by poling. In the poling process will the material be heated to above its Curie temperature, causing the PZT to assume centrosymmetric lattice structure and loose all polarization, as seen to the left in figure 2.5. Then a strong electric field is applied across the material and the temperatures is lowered while the field is still applied. This forces the polarization in the unit cells to align to the exterior field, resulting in a strong polarization of the bulk material.
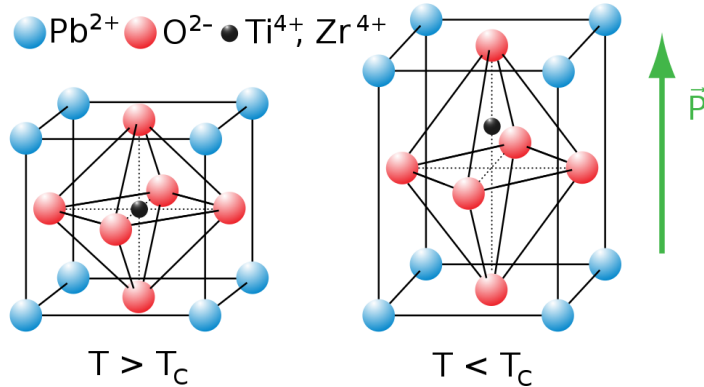
Figure 2.5: Crystal structure of PZT, above and below its Curie temperature (T_C) [20].

2.2.2 Mathematical description

A piezoelectric material is described by both the laws of mechanics and those of electromagnetics, for this reason it is prudent to get an overview of the relevant laws of both domains before attempting to combine them.

The mechanical properties of a piezoelectric material can, assuming only small deformation, be described as a linear-elastic material. Consequently it follows the generalized Hooke's law, as seen in eq 2.2. Electrically, a piezo-electric material is a polarizable dielectric. Hence, the electrical behaviour of the material is as described in eq 2.19.

$$\begin{bmatrix} D_1 \\ D_2 \\ D_3 \end{bmatrix} = \epsilon_0 \begin{bmatrix} E_1 \\ E_2 \\ E_3 \end{bmatrix} \begin{bmatrix} P_1 \\ P_2 \\ P_3 \end{bmatrix}, \qquad \nabla \cdot \boldsymbol{D} = 0 \qquad (2.19)$$

Where $\boldsymbol{D}$ is the electric displacement field, $\boldsymbol{\epsilon_0}$ is the vacuum permittivity, $\boldsymbol{E}$ is the electric field and $\boldsymbol{P}$ is the polarization density. While the second equation defines the material as a dieelectric, i.e. no free charges. The index convention is the same as with the first three values in the stress and strain vectors.

The piezoelectric effect is, as previously mentioned, a linear effect. This implies that eqs 2.2 and 2.19 can be expanded with a linear term to include said effect. For instance will the stress in a piezoelectric material expressed by the strain and electric field be as seen in eq 2.20, while the electric displacement field expressed by the strain and the electric field will be as seen in eq 2.21. These equations give a mathematical expression for the inverse

9

and direct piezoelectric effect, respectively.

$$
\begin{bmatrix} T_1 \\ T_2 \\ T_3 \\ T_4 \\ T_5 \\ T_6 \end{bmatrix} = \begin{bmatrix} c_{11}^E & c_{12}^E & c_{13}^E & c_{14}^E & c_{15}^E & c_{16}^E \\ c_{21}^E & c_{22}^E & c_{23}^E & c_{24}^E & c_{25}^E & c_{26}^E \\ c_{31}^E & c_{32}^E & c_{33}^E & c_{34}^E & c_{35}^E & c_{36}^E \\ c_{41}^E & c_{42}^E & c_{43}^E & c_{44}^E & c_{45}^E & c_{46}^E \\ c_{51}^E & c_{52}^E & c_{53}^E & c_{54}^E & c_{55}^E & c_{56}^E \\ c_{61}^E & c_{62}^E & c_{63}^E & c_{64}^E & c_{65}^E & c_{66}^E \end{bmatrix} \begin{bmatrix} S_1 \\ S_2 \\ S_3 \\ S_4 \\ S_5 \\ S_6 \end{bmatrix} - \begin{bmatrix} e_{11} & e_{21} & e_{31} \\ e_{12} & e_{22} & e_{32} \\ e_{13} & e_{23} & e_{33} \\ e_{14} & e_{24} & e_{34} \\ e_{15} & e_{25} & e_{35} \\ e_{16} & e_{26} & e_{36} \end{bmatrix} \begin{bmatrix} E_1 \\ E_2 \\ E_3 \end{bmatrix} \quad (2.20)
$$

$$
\begin{bmatrix} D_1 \\ D_2 \\ D_3 \end{bmatrix} = \begin{bmatrix} e_{11} & e_{12} & e_{13} & e_{14} & e_{15} & e_{16} \\ e_{21} & e_{22} & e_{23} & e_{24} & e_{25} & e_{26} \\ e_{31} & e_{32} & e_{33} & e_{34} & e_{35} & e_{36} \end{bmatrix} \begin{bmatrix} S_1 \\ S_2 \\ S_3 \\ S_4 \\ S_5 \\ S_6 \end{bmatrix} - \begin{bmatrix} \epsilon_{11}^S & \epsilon_{12}^S & \epsilon_{13}^S \\ \epsilon_{21}^S & \epsilon_{22}^S & \epsilon_{23}^S \\ \epsilon_{31}^S & \epsilon_{32}^S & \epsilon_{33}^S \end{bmatrix} \begin{bmatrix} E_1 \\ E_2 \\ E_3 \end{bmatrix} \quad (2.21)
$$

The superscripted E's in eq 2.20 indicate that the values of the stiffness matrix were measured while the electric field across the material was constant. Similar superscripts exist to indicate constant electric displacement field, stress or strain. A permittivity matrix, $\boldsymbol{\epsilon}$, has also been introduced to replace the vacuum permittivity and the polarization vector. And it has been necessary to include the $\boldsymbol{e}$-coefficients. These are one of four sets of piezoelectric coefficients used to relate the mechanical ($\boldsymbol{S}$ and $\boldsymbol{T}$) and the electrical variables ($\boldsymbol{E}$ and $\boldsymbol{D}$). All these relations are listed in their abbreviated form in eq 2.22 giving four different sets of piezoelectric parameters.

$$
\boldsymbol{D} = \boldsymbol{eS} + \boldsymbol{\epsilon}^S \boldsymbol{E} \qquad (2.22a)
$$
$$
\boldsymbol{T} = \boldsymbol{c}^E \boldsymbol{S} - \boldsymbol{e}^t \boldsymbol{E} \qquad (2.22b)
$$

$$
\boldsymbol{D} = \boldsymbol{dT} + \boldsymbol{\epsilon}^T \boldsymbol{E} \qquad (2.22c)
$$
$$
\boldsymbol{S} = \boldsymbol{s}^E \boldsymbol{T} + \boldsymbol{d}^t \boldsymbol{E} \qquad (2.22d)
$$

$$
\boldsymbol{E} = -\boldsymbol{gT} + (\boldsymbol{\epsilon}^T)^{-1} \boldsymbol{D} \qquad (2.22e)
$$
$$
\boldsymbol{S} = \boldsymbol{s}^D \boldsymbol{T} + \boldsymbol{g}^t \boldsymbol{D} \qquad (2.22f)
$$

$$
\boldsymbol{E} = -\boldsymbol{hS} + (\boldsymbol{\epsilon}^S)^{-1} \boldsymbol{D} \qquad (2.22g)
$$
$$
\boldsymbol{T} = \boldsymbol{c}^D \boldsymbol{S} - \boldsymbol{h}^t \boldsymbol{D} \qquad (2.22h)
$$

The superscripted t in some of these equations indicate that the matrix is transposed, while the $\boldsymbol{s}$-matrix is the compliance matrix of the material, which is the inverse of the stiffness matrix. Each of these sets of parameters

10

gives a mathematical description of the direct and the inverse piezoelectric effect in the upper and lower equation respectively, and is sufficent to descibe the material. Each of the four sets are also related to each other, hence it is possible to change from one set of parameters to another if it should become necessary.

2.2.3 Symmetries in PZT

Eqs 2.20 and 2.21 contains a large number of independent variables, 63 in total. However, this number is significantly reduced when including the symmetry in PZT. The poling process will turn PZT into a transversely isotropic material with a rotational symmetry around the direction of polarization, usually defined as the x_3-direction[28]. One of the parametric sets for such a material can be written as seen in eqs 2.23 and 2.24, showing that the number of independant variables has been reduced to 10.

$$\begin{bmatrix} T_1 \\ T_2 \\ T_3 \\ T_4 \\ T_5 \\ T_6 \end{bmatrix} = \begin{bmatrix} c_{11}^E & c_{12}^E & c_{13}^E & 0 & 0 & 0 \\ c_{12}^E & c_{11}^E & c_{13}^E & 0 & 0 & 0 \\ c_{13}^E & c_{13}^E & c_{33}^E & 0 & 0 & 0 \\ 0 & 0 & 0 & c_{44}^E & 0 & 0 \\ 0 & 0 & 0 & 0 & c_{44}^E & 0 \\ 0 & 0 & 0 & 0 & 0 & c_{66}^E \end{bmatrix} \begin{bmatrix} S_1 \\ S_2 \\ S_3 \\ S_4 \\ S_5 \\ S_6 \end{bmatrix} - \begin{bmatrix} 0 & 0 & e_{31} \\ 0 & 0 & e_{31} \\ 0 & 0 & e_{33} \\ 0 & e_{15} & 0 \\ e_{15} & 0 & 0 \\ 0 & 0 & 0 \end{bmatrix} \begin{bmatrix} E_1 \\ E_2 \\ E_3 \end{bmatrix} \quad (2.23)$$

Where $c_{66}^E = \frac{1}{2}(c_{11}^E - c_{12}^E)$.

$$\begin{bmatrix} D_1 \\ D_2 \\ D_3 \end{bmatrix} = \begin{bmatrix} 0 & 0 & 0 & 0 & e_{15} & 0 \\ 0 & 0 & 0 & e_{15} & 0 & 0 \\ e_{31} & e_{31} & e_{33} & 0 & 0 & 0 \end{bmatrix} \begin{bmatrix} S_1 \\ S_2 \\ S_3 \\ S_4 \\ S_5 \\ S_6 \end{bmatrix} - \begin{bmatrix} \epsilon_{11}^S & 0 & 0 \\ 0 & \epsilon_{11}^S & 0 \\ 0 & 0 & \epsilon_{33}^S \end{bmatrix} \begin{bmatrix} E_1 \\ E_2 \\ E_3 \end{bmatrix} \quad (2.24)$$

2.3 Loss

All materials are in some way lossy, this includes piezoelectric materials where three different types of losses occur, namely dielectric, mechanical and piezoelectric loss[26]. These can all be included into calculations through the use of complex permittivity, stiffness matrix and piezoelectric coefficient, respectively. However, in this thesis is only mechanical loss implemented in the simulations.

The attenuation of a mechanical wave is caused by a combination of power absorpsion and and scattering, however the former is most prominent [22].

This attenuation is usually included into the system as a complex elastic stiffness:

$$c^* = c' - jc'' = c'(1 - j \cdot tan\delta_m) = c'(1 - \frac{j}{Q_m}) \qquad (2.25)$$

Where c' and c'' are the real and imaginary stiffness, respectively. While $tan\delta_m$ is the mechanical loss tangent and the invers of the mechanical Q-factor, Q_m.

2.4 Finte element method

The behavior of a physical system is usually governed by some boundary conditions and a set of equations, some of them partial differential (PDE). Direct analysis of such a system can be very difficult, especially if the structure is complicated. However, the finite element method (FEM) can solve physical systems of imense complexity through approximations of the PDEs and dicretization of the system geometry.

The method is generally performed as in the following steps:

1. Governing equations of the system are identified, and an approximation is derived.

2. The system is discretized into a finite number of elements.

3. An approximation of the dependent variable is introduced in each element.

4. The integral form equation is evaluated for each element.

5. The solution in each element is assembled as a global matrix equation.

6. Said matrix equation is solved.

7. Values of interest can be calcuated from the solution of the matrix.

2.4.1 Elements and nodes

Each domain in a physics model will in the finite element method be divided into elements [14]. These elements are usually polygons with three or four corners, but elements with curved sides can be introduced in order to follow curved domain boundaries. There is always a node at each corner of the element, and often one or more nodes equally spaced along the sides. For the simulations in this thesis was a triangular element with a midside node, also

(a) Mesh.

(b) Nodal placements in a quadratic triangular element.
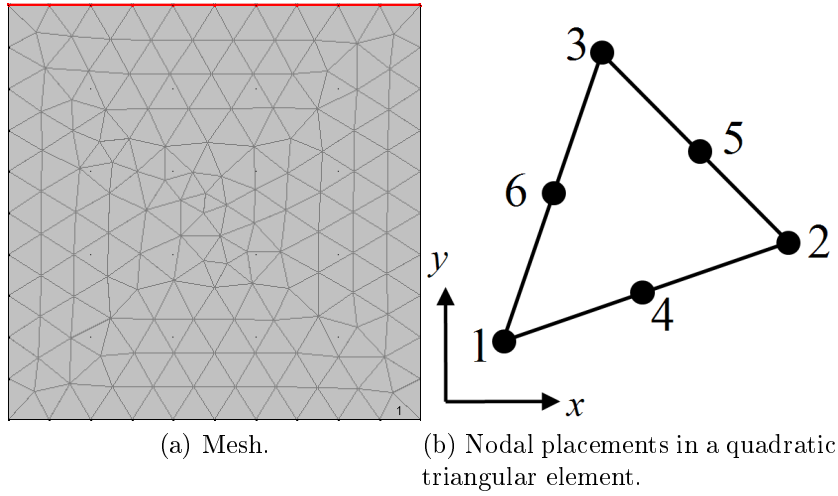
Figure 2.6: Triangluar element

known as a quadratic triangular element, consistently used. For this reason is it depicted in figure 2.6 and used as an example in this section. For each of the six nodes in this element, will there be defined a shape function N_i that is unity at node i, but zero at all other nodes and defined as zero outside of the element. In addition will the sum of all the shape functions be at unity anywhere within an element. These conditions will in this element cause the shape functions to be quadratic functions of the coordinates, giving rise to the name quadratic triangular element. These functions are then, along with the nodal values of the dependent variable $\tilde{\boldsymbol{u}}_a$, used to obtain the approximate value of the dependent variable, $\hat{\boldsymbol{u}}$, anywhere within the element:

$$\boldsymbol{u} \approx \hat{\boldsymbol{u}} = \sum_{a=1}^{n} \boldsymbol{N}_a \tilde{\boldsymbol{u}}_a \qquad (2.26)$$

With n being the number of nodes in the element (in this case 6) and $\boldsymbol{u}$ being the exact value of the dependent variable. It must be noted that $\tilde{u}_i$ is a vector only if there is more than one dependant variable. For example as in solid mechanics, where the dependent variables are the displacements in x, y and z-direction. This interpolation is a good approximation for variables as long as said variable is constantly increasing or decreasing inside an element. Which implies that the sinusoidal variations associated with a wave will require several elements per wavelength to obtain a good approximation. In this thesis has six elements per wavelength been set as the lowest acceptable resolution.

13

2.4.2 Integral form of partial differential equations

The derivation of integral forms of partial differential equations is an extensive topic, and will not be presented in detail here. However, a brief outline will be given [18].

In a physics problem governed by differential equations is the function $\boldsymbol{u}$ sought after. This function will satisfy a set of differential equations, $\boldsymbol{A}(\boldsymbol{u})$, anywhere within the system or domain, Ω, and a set of conditions, $\boldsymbol{B}(\boldsymbol{u})$ on the boundary, Γ, of said domain. The equations and conditions can be expressed as:

$$\boldsymbol{A}(\boldsymbol{u}) = \left\{ \begin{array}{c} A_1(\boldsymbol{u}) \\ A_2(\boldsymbol{u}) \\ \vdots \end{array} \right\} = \boldsymbol{0} \qquad \boldsymbol{B}(\boldsymbol{u}) = \left\{ \begin{array}{c} B_1(\boldsymbol{u}) \\ B_2(\boldsymbol{u}) \\ \vdots \end{array} \right\} = \boldsymbol{0} \qquad (2.27)$$

In the finite element method is however the system discrete, so the approximate value of $\boldsymbol{u}$ is only defined in a finite number of nodes. And as all the shape functions are zero outside of its respective element, it indicates that eq 2.26 is valid across the entire domain, when n is set as the total number of nodes, instead of that of just one element. Some of the nodal values, $\tilde{\boldsymbol{u}}_a$, might be known through the boundary conditions, but the absolute majority is unknown. The objective is then to find functions or operators $\boldsymbol{G}_b$ and $\boldsymbol{g}_b$ so that:

$$\int_\Omega \boldsymbol{G}_b(\hat{\boldsymbol{u}}) d\Omega + \int_\Gamma \boldsymbol{g}_b(\hat{\boldsymbol{u}}) d\Gamma = 0, \quad b = 1, 2, 3, ..., n \qquad (2.28)$$

This equation can, due to the nature of finite integral, also be written as:
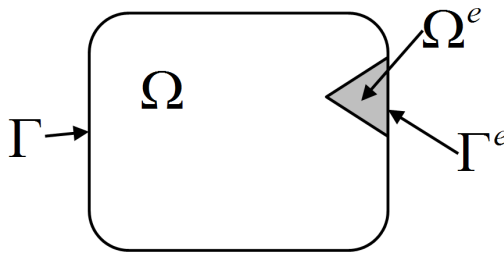
Figure 2.7: The domain Ω with an element Ω^e, boundary Γ and element boundary Γ^e.

$$\sum_{e=1}^{m} \left(\int_{\Omega^e} \boldsymbol{G}_b(\hat{\boldsymbol{u}}) d\Omega + \int_{\Gamma^e} \boldsymbol{g}_b(\hat{\boldsymbol{u}}) d\Gamma \right) = 0, \quad e = 1, 2, 3, ..., m \qquad (2.29)$$

Here is Ω^e the area of a single element and Γ^e is the boundary of that same element. It is also assumed that the m elements cover the entire domain Ω. This implies that the integral can be calculated in every element, and then summed up to yield an approximate solution for the entire domain. Thus giving the the value of $\hat{\boldsymbol{u}}$ in every node.

Given the definition of $\boldsymbol{A}(\boldsymbol{u})$ in eq 2.27 it is clear that:

$$\int_\Omega \boldsymbol{v}^T \boldsymbol{A}(\boldsymbol{u}) d\Omega = 0 \qquad (2.30)$$

Where $\boldsymbol{v}$ is a set of n arbitrary test functions. The same conclusion can be made for the boundary condition with the test functions $\bar{\boldsymbol{v}}$ that are defined on the boundary. This equation is however, not valid when $\boldsymbol{u}$ is approximated. Still, if the test functions are replaced by weighting functions, then eq 2.30 and its boundary counterpart will become valid once more. In the Galerkin method, which is the one used by COMSOL, are these weighting functions identical to the shape functions. Thus yielding:

$$\int_\Omega \boldsymbol{N}_b^T \boldsymbol{A}(\hat{\boldsymbol{u}}) d\Omega + \int_\Gamma \boldsymbol{N}_b \boldsymbol{B}(\hat{\boldsymbol{u}}) d\Gamma = 0, \quad b = 0, 1, 2, 3, ..., n \qquad (2.31)$$

This equation is on the same form as eq 2.28, and can be applied for the evaluation in each element.

Chapter 3

Equipment

3.1 Xtrans

Xtrans is a MATLAB program employing the Mason model[15] to preform a one-dimentional analysis of piezoelectric transducers. It has in this thesis been used to confirm the validity of the simulations in COMSOL through a direct comparison of results.

The program can handle a large stack of piezoelectric and matching layers, however only one of each were necessary in the in the models that were used in this thesis. Each layer is defined as a certain material by stating the characteristic acoustic impedance, longitudinal wave speed and mechanical Q-factor. Any piezoelectric layer will in addition to these parameters require the piezoelectric coefficient, h_{33}, and the relative clamped permittivity, $\epsilon_{33}^S/\epsilon_0$, assuming that the piezoelectric material is poled in the 3-direction. Finally must the thickness of each layer be set, exept for the backing and load as these are assumed to be infinitely thick.

For the model used in this thesis (one piezoelectric and one matching layer) will the program compile a three dimentional matrix of the size $2\times2\times n$, with n being the number of frequencies the analysis was performed for. The standard settings will do this for frequencies from 1kHz to 20MHz with a stepsize of 1kHz, resulting in a n of 20000. This matrix can also be described as a 2×2 that will vary as a function of frequency, and has a form as follows:

$$\begin{bmatrix} Y & H_{tt} \\ H_{tt} & Y_M \end{bmatrix} \tag{3.1}$$

Where Y is the electrical admittance per area of the transducer, H_{tt} is the average surface velocity divided by the voltage and Y_M is the mechanical admittance[25].

Xtrans has been developed at the Department of circulation and medical imaging at NTNU.

3.2   COMSOL Multiphysics

COMSOL Multiphysics 4.0a, from here on refered to as COMSOL, is a simulation program that employs the finite element method to solve complex physics problems governed by PDEs. The program is designed to offer all the customization desired by an advanced user, while being relatively easy to get started with for an inexperienced user. This in mainly due to the preset physics interfaces, which can be used to include the governing equations from a wide variety of physics problems into a model. However, an advanced user is at liberty to mathematically define a custom physics interface from scratch. A single model can include and couple several physics interfaces to allow for interactions that are often observed in the real world. Some of these coupled situations also exist as predefined physics interfaces, such as the Piezoelectric Devices interface, which is a combination of solid mechanics and electrostatics.

A full description of COMSOL in this thesis would be impractical and highly unneccesary. However, a short description of the applied features is included, to give an insight to the modelling procedures. The usual construction of a model includes the following steps:

1. Select the number of space dimentions in the model, chose one or more physics interfaces and decide the study type. This is done in a built-in wizard at the start of every new model. In this thesis were the pressure acoustics and piezoelectric devices interfaces and a frequency domain study type used for all simulations.

2. Import the geometry of the model, or draw it with the built-in CAD tools.

3. Set which of the domains that are governed by each of the physics interfaces. A single domain might be governed by several interfaces in a multiphysics model.

4. Apply correct conditions to domains and boundaries in the model. Each physics interface has a series of standard conditions that are automatically applied to the domains governed by it, and any manually applied conditions will replace these.

5. Assign materials to the domains in the model. Many materials are included in COMSOL, but custom materials can also be implemented and saved for later use.

6. Mesh the model. Distribution, size and type of elements can be set. Alternatively can the standard free triangular mesh can be applied with predefined element sizes ranging from extremely coarse to extremely fine.

7. Study settings are decided, such as what range of frequencies a frequency domain model should be solved for.

8. COMSOL solves the problem, and the user can study the solution through a selection of post-processing and/or visualization techniques.

3.2.1 Geometry

The shape of the model and its domains can be built from a selection of basic geometric shapes with the included CAD features. This allows for practically any geometric shape to be designed through transformations and boolean operations. All the steps in the drawing process is kept as a sequence, thus making it easy to go back and do changes. In addition can the use of global parameters during drawing give a final model with dimentions that are easy to change. An example of such a parameter is be the thickness of the various layers in a piezoelectric transducer.

3.2.2 Pressure acoustics

In the pressure acoustics physics interface is the pressure, p, the only dependent variable. And the governing PDE is:

$$\nabla \cdot \left(-\frac{1}{\rho_0}(\nabla p - \mathbf{q}) \right) - \frac{\omega^2 p}{\rho_0 c^2} = Q \tag{3.2}$$

Where $p(\mathbf{x}, t) = p(\mathbf{x})e^{i\omega t}$, ρ_0 is the density, c is the speed of sound and $\mathbf{q}$ and Q are dipole and monopole sources, respectively[5]. These sources are not present in the models in this thesis, thus allowing for the PDE to be simplified. The various features and conditions applied to the interface are briefly described in the following list.

Pressure Acoustics Model must be applied to all domains governed by the interface. Here can the fluid model be set, for example viscous or linear elastic, the latter being used in the models in this thesis unless

explicitly mentioned. Temperature and absolute pressure is also set here, the standard being room temperature and one atmosphere. Based on these settings will the model give the governing equations for the domains. Models with different settings can be used for the different domains if necessary.

Sound Hard Boundary (Wall) is the standard condition for all boundaries governed by the pressure acoustics interface. It sets the normal acceleration on the boundary to zero, thus emulating a wall.

Inital Values allows for initial pressure and pressure time derivative to be set in the domains. In this thesis were all initial values set to 0.

Axial Symmetry is a default boundary condition for axisymmetrical simulations, where it is used to define said symmetry. It is automatically set as a condition on all boundaries that lie along the line where $R = 0$.

Normal Acceleration overides the standard condition on the boundaries where it is applied, by setting an acceleration that can be defined as directed inwards normal to the boundary or in terms of the coordinates x and y. This condition is used to couple acoustic domains to adjacent mechanical domains through a preset (`pzd/pzm1`) that sets the acceleration on the boundary of the latter as the condition.

3.2.3 Piezoelectric devices

The piezoelectric devices interface is, as previously mentioned, a combination of the solid mechanics and electrostatics interfaces. Consequently are the dependent variables the electric potential, V, and the three components of the displacement, x, y and z. And the governing equations are as seen in 2.22, where the relation between strain and displacement is given by eq 2.1 while the electric potential is related to the electric field as:

$$\boldsymbol{E} = -\nabla\boldsymbol{\Phi} \tag{3.3}$$

Where $\boldsymbol{\Phi}$ is the electric potential[5]. The equations are adapted to a frequency domain study by converting the dependent variable to harmonic complex variables [17]:

$$\boldsymbol{u}(\boldsymbol{x},t) = \boldsymbol{u}(\boldsymbol{x})e^{j\omega t} \qquad \Phi(\boldsymbol{x},t) = \Phi(\boldsymbol{x})e^{j\omega t} \tag{3.4}$$

Here is $\boldsymbol{u}$ a vector consisting of the three displacement components. All features and conditions that are applied to this interface are described in the following list.

Piezoelectric material model must, in the same way as in the acoustic interface, be applied to all domains governed by the piezoelectric interface. Also here is the temperature and absolute pressure set, with the same standard values as in the acoustics. A feature in this model is the possibility to align the model with an other coordinate system than the global cartesian system. This is often necessary, as piezoelectric materials are generally defined to be poled in the 3-direction, which coincide with the z-direction in the global system. A two-dimentional model is however set in the x-y plane, causing the piezoelectric to be poled in the out-of-plane direction.

Free is the standard mechanical boundary condition, and therefore initially applied to all boundaries in domains governed by the piezoelectric interface. It defines the boundary as free to move in any direction, and without any loads acting on in.

Zero charge is the default electrostatic boundary condition. It defines, as the name implies, that there is no electric charge on the boundary.

Initial values gives the option of setting an initial displacement field, velocity field, electric potential or time derivative of said potential in any of the domains governed by the piezoelectric interface. All intital values were set as zero in this thesis.

Axial symmetry is only available in the axisymmetrical models, where it defines the axis of symmetry. It is set as a standard condition on all boundaries that lie along the line where $R = 0$.

Electric potential sets the electrical potential to a given value on the boundary the condition is applied to.

Ground sets the electrical potential to zero at the boundary it applies to.

Symmetry indicates that the model is a part of a larger structure that is mirror symmetrical around the boundary where this condition is applied, and thus overrides the free boundary condition. In this thesis is the symmetry conditions used on both sides of a 2D model to emulate a theoretical transducer that is infinite in the directions perpendicular to the symmetry plane.

Roller suppresses the standard mechanical condition, and defines that there can be no displacement perpendicular to the boundary, but tangential displacement is still allowed.

21

Damping and Loss allows for the inclusion of dielectric, mechanical and piezoelectric damping in the various domains. The loss factors can be set in this feature, and thus apply to all domains with loss. Alternatively can they be set in each material as a property that is only included when required.

Boundary load is also a condition that replaces the standard free condition. It states that a given mechanical load is applied on the boundary. This can be used to couple a mechanical domain to a bordering acoustic domain by setting the pressure in the acoustic domain as a force per unit area on the boundary of the mechanical domain. A preset exists to simplify the application.

3.2.4 Materials

COMSOL includes, as previously mentioned, a large library of pre-defined materials, and additional ones can be made with any of these materials as a basis or from the ground up. When a material is applied to a domain will COMSOL perform a check to see if the selected material includes all the specifications that are required by the physics models governing the domain. If this is not the case, will a notification be given, and the user must add the requested specifications to the model or change the material. For the pressure acoustics model model with a linear elastic fluid model can the required material specifications be set as either speed of sound and density, or impedance and wavenumber. The former is used for all simulations in this thesis. While the piezoelectric material model will, for the stress-charge form of the equations, require the elasticity matrix $\boldsymbol{c}^E$, $\boldsymbol{e}$-coefficients, relative permittivity $\boldsymbol{\epsilon}^S/\epsilon_0$ and density ρ. Alternatively can the strain-charge form be used, but this was not done in any of the simulations in this thesis. All necessary specifications for the materials used in this thesis can be found in appendix A.

3.2.5 Perfectly matched layer

In many physics problem involving waves will the aforementioned waves be generated in or enter an area of interest and later disappear out of said area toward infinity. In contrast, is the size of a finite element model definitely not infinite, resulting in waves being reflected on the outer boundaries of the model. However, this problem can be adequately solved with the use of a perfectly matched layer[3], from here on referred to as a PML. This layer introduces a coordinate transformation, causing the resulting coordinate to

be complex, see figure 3.1 (a) and (b) for a illustration. This transform will cause the PML to act as a material where the loss factor increases as a function of the position. It will therefore dampen the wave, e^{ikx}, at an exponential rate, while not causing any reflections on the boundary of the PML. It can from figure 3.1 be concluded that an increase in the growth

(a) Real and imaginary part of x in regular space

(b) Real and imaginary part of x when entering the PML.

(c) The wave e^{ikx} in regular space.

(d) The wave e^{ikx} when entering the PML
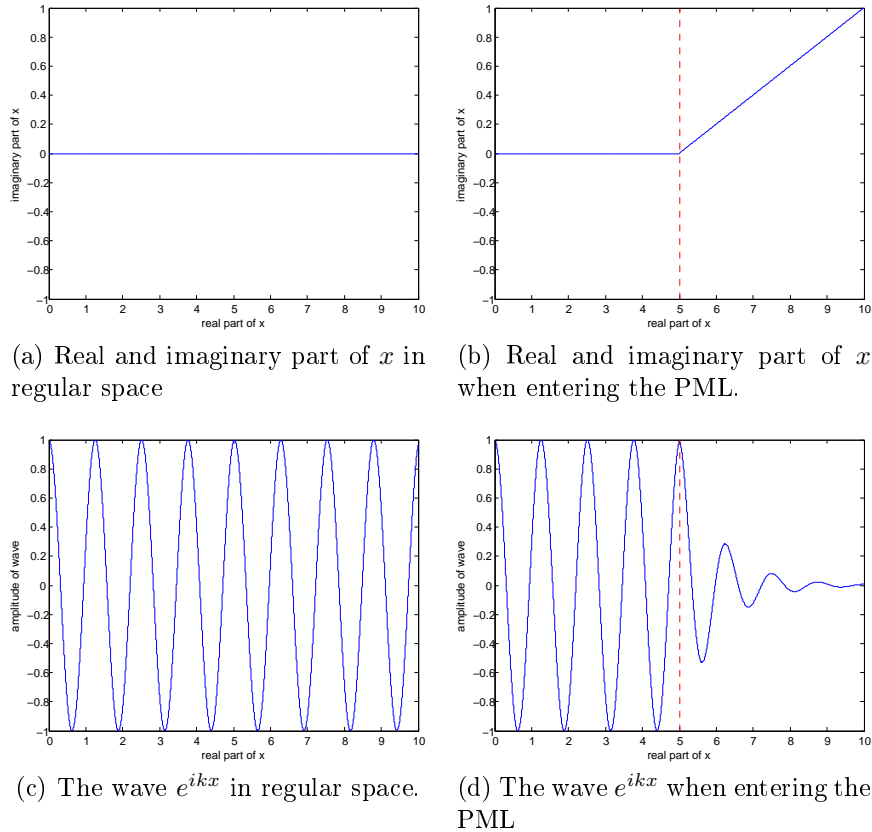
Figure 3.1: General consept of a PML, shown with x as coordinate and the red dashed line indicating the boundary between regular space and the PML.

rate of the imaginary part of x will cause the wave to be absorbed over a shorter distance. Thus allowing for thinner PMLs, eventually resulting in a infinitesimal thickness. This is however not the case in FEM, where approximations are used in stead of the actual wave equation[12]. It should also be noted that the transformation in only performed for one coordinate, and as a consequence will the attenuation rate be dependent on the direction of the wave.

The PMLs in the acoustic and piezoelectric interfaces of COMSOL are implemented in two different ways. As a result is the acoustic PML capable of adapting to to the current wavelength in the medium during a frequency

domain simulation, while the piezoelectric PML must be given a constant wavelength for it to match, making it less suited for a frequency sweep over a large range. However, this problem can be circuvented by setting the matched wavelength to: `pzd.cp/freq`, which is the speed of a pressure wave in the PML as caluated by COMSOL, divided by the current frequency. It should also be noted that in the piezoelectric interface is the domain of the PML automatically set to be isotropic, and will thus require values to be set for Young's modulus and Poisson's ratio in the material model.

3.2.6 Meshing and solving

The free triangular mesh was used in all simulations, with all parameters exept the element size kept at the values decided by the program. The order of the shape functions can be set in each physics interface, ranging from linear to quintic. They were however intially set as quadratic for all the dependent variables in this thesis, and kept as such troughout the simulations. All simulations were solved with standard settings for the solvers, and frequencies ranging from 100kHz to 20Mhz with a step of 100kHz, this will from here on be referred to as the standard frequency range.

3.2.7 Post-processing

Data was extracted from the solved models with the help of average operators in the two-dimentional models, and through line integrals in the two-dimentional axisymmetric models. An average operator is used to obtain the average value of any available physical quantity in a domain or at boundary for each step in a simulation with a parametric sweep. After the simulation can the value be used to calculate derived values, which can then be displayed along with the parameter values in a spreadsheet, or plotted as a function of said parameter value in a global plot.

In the two-dimentional simulations in this thesis were two average operators used, one was connected to the boundary between the piezoelectric layer and the matching layer (`aveop1`), while the other (`aveop2`) was connected between the matching layer and the load. The values from these operators were used to derive the admittance and Htt of the transducer relative to the frequency in each simulations through the expressions listed in table 3.1. In the two-dimentional axisymmetrical models could the average operators however not be used, as they would not account for the rotational symmetry. As previously mentioned were instead line integrals used on the appropriate boundaries. An option for the line integral in an axisymmetrical model is to automatically compute the surface integral of the rotated surface instead of

Expression	Derived value
`aveop1(real(pzd.nJ))/(100[V])`	Real part of admittance
`aveop1(imag(pzd.nJ))/(100[V])`	Imaginary part of admittance
`aveop2(real(pzd.u_tY))/(100[V])`	Real part of Htt
`aveop2(imag(pzd.u_tY))/(100[V])`	Imaginary part of Htt

Table 3.1: Expression used to extract admittance and Htt from COMSOL. `pzd.nJ` is the current density normal to the boundary where `aveop1` is applied, while `pzdu_tY` is the velocity in the y-direction of the boundary where `aveop2` is applied. `100[V]` is the applied electric potential of 100V.

the line, this was employed in all axisymmetrical models in order to simplify the integrals.

All resulting data was exported from COMSOL and added to an excel-spreadsheet. This was then imported into Matlab, where a side by side comparison could be made to the results from Xtrans.

Chapter 4

Simulations

4.1 Plane water-loaded PZT-5H plate with epoxy matching layer

4.1.1 Modeling

The first finite element model of a piezoelectric transducer was designed to familiarize with COMSOL Multiphysics, and to create a model with results that could easily be compared with those of Xtrans. All basic knowledge required to make this model was obtained by studying the built-in tutorial of a piezoacoustic transducer [6]. The model consist, as seen in figure 4.1, of four domains where two are solved with the Piezoelectric device interface (pzd) and the other two with the pressure acoustics interface (acpr). The characteristics of each domain is listed in table 4.1. In addition was domain

Domain	1	2	3	4
Width	2.5mm	2.5mm	2.5mm	2.5mm
Thickness	0.125mm	0.08mm	2mm	2mm
Physics interface	pzd	pzd	acpr	acpr
Material	PZT-5H	epoxy	water	water

Table 4.1: Descriptions of the domains in the first simulation. Material data for PZT-5H, epoxy and water is found in appendix A.

4 defined as a PML to prevent reflections from the load, while a backing layer with zero compressibility was achieved by applying a a roller condition to the lower boundary of domain 1. This is also achieved in Xtrans by setting an extremely high impedance in the backing layer (100000 MRayl was used in this case). The material properties for PZT-5H defines the poled direction to
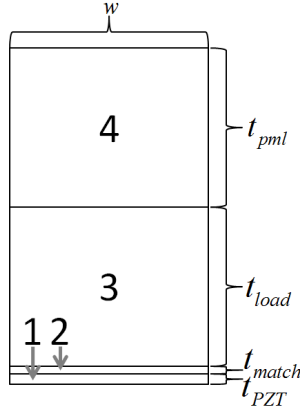
Figure 4.1: Geometry of the model, w = width of model, t_{PZT} = thickness of piezoelectric layer, t_{match} = thickness of matching layer, t_{load} = thickness of load layer, t_{PML} = thickness of perfectly matched layer.

be in the 3-direction, which coresponds with the out of plane direction in the global coordinate system for a two-dimentional model. This was corrected by orienting the piezoelectric material after a different coordinate system, which is defined in table 4.2. The model was initially intended to describe a

Global coordinate system	X	Y	Z
Base vector system	x1	x3	x2

Table 4.2: Base vector system applied to align poling direction of PZT-5H (x3) to global Y-axis.

single element transducer with a width of 2.5mm, but symmetry conditions was later applied to the left and right boundaries of domains 1 and 2 to emulate a transducer with infinitely large lateral dimentions. Thus causing the model behaviour to be very close to that of a 1-D model. Furthermore were the electrical boundary conditions of ground and an electric potential of 100V applied to the upper and lower boundaries of domain 1, respectively. The connection between the acoustic and peizoelectric device interfaces was made with a normal acceleration condition applied to the lower boundary of domain 3, and a boundary load condition to the upper boundary of domain 2 as descibed in section 3.2. It is also important to notice that this model is lossless, which can be implemented in Xtrans by setting very high values of Q (10000 was used for this simulation). Finally, were average operators attached to the boundaries between domains 1 and 2, and between 2 and 3.

The meshing of domains 3 and 4 was done with the standard free trian-

gular mesh, and the element size was set to the predefined value of extremely fine. This resulted in a maximum and minimum element size limited to 42.1μm and 0.0841μm, respectively, and a total of 16435 elements. Domains 1 and 2 were meshed with the same type of mesh, but the size limits of the elements were halved, giving a total of 2004 elements. This variation in mesh sizes was done to increase the resolution in the thin piezoelectric domains, while keeping the number of elements in the acoustic domains at a manageble level.

After meshing was the model solved in the frequency domain for the standard frequency range. This range gives the same maximum frequency as the regular frequency range of Xtrans, but in the latter is both the starting frequency and the step size 1kHz.

4.1.2   Results and discussion

The admittance of the piezoelectric layer and the average velocity on the matching layer to load boundary was obtained from both COMSOL and Xtrans as described in 3.2.7 and the corresponding variables were plotted together as seen in figure 4.2. These plots show that the results from the two simulation programs are close to identical, and the minute differences are only visible when observing a small sections of the plots (fig 4.3). Nonetheless is this not a good model for a large portion of the frequency range. The cause of this is the relatively large element size, which will be too big for frequencies above 5.8Mhz in the water and 9.5MHz in the epoxy when enforcing the minimum resolution of six elements per wavelength. This problem can be seen in figure 4.5 (a) where the pressure in the load is plotted at 20MHz. Still the results obtained from the finite element model are very similar to those from Xtrans, which could lead to the erroneous conclusion that the element size is not that important. The good results are however, probably caused by the fact that the evaluated values are obtained by calculating the mean value of all the nodes along a boundary. If the nodal values are assumed to in some degree to vary randomly around the true value, then the mean value will be close to the true mean value if there is a sufficiently high number of nodes. This implies that the accuracy of the results can in this case be attributed to the size of the model.

(a) Real part of admittance   (b) Imaginary part of admittance

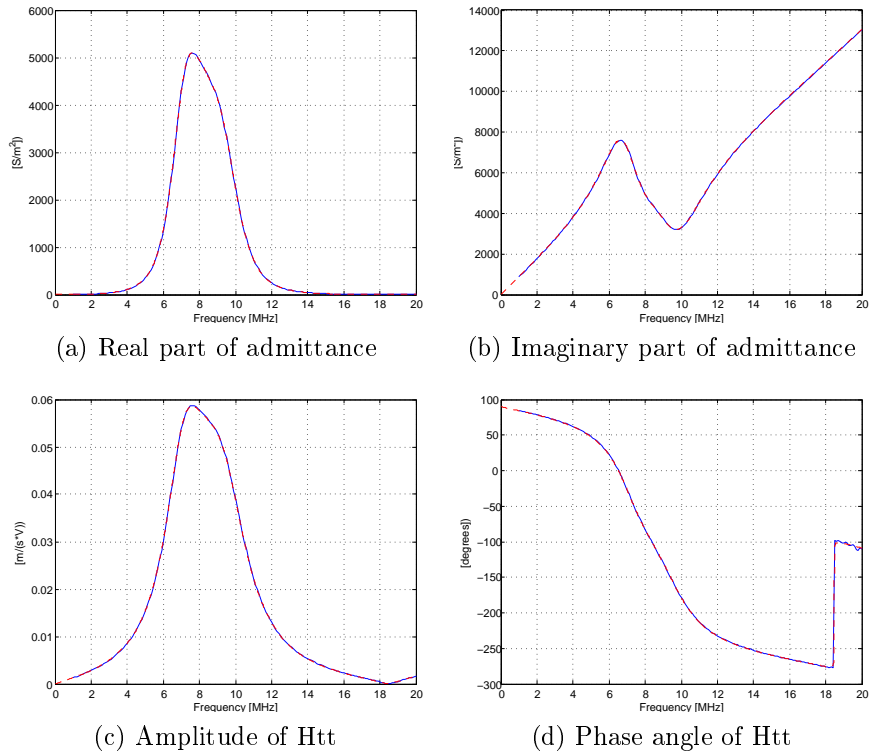(c) Amplitude of Htt   (d) Phase angle of Htt

Figure 4.2: Admittance and Htt found in COMSOL (blue line) and Xtrans (red, dashed line) for the first model.
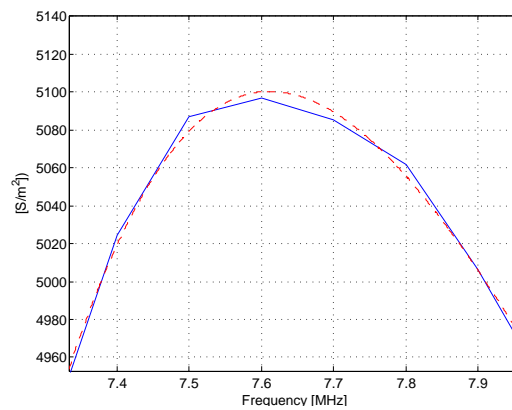

Figure 4.3: A small section of fig 4.2 (a), showing the difference between the results from COMSOL and Xtrans.

4.2   Refinement of model

4.2.1   Modeling

The model in the previous section proved to give results very similar to those of the one-dimentional model in Xtrans, but it was a fairly large model with many elements, despite their large size. It was therefore required to reduce the size of the model, both to shorten calculation time and to reduce the element size to less than one sixth of the smallest wavelength. This could easily be done to the model with its current boundary conditions. Reducing the width of the model would ideally have no effect because of the symmetry conditions, and the load layer and PML could be reduced as long as the PML continued to effectively absorb the pressure wave.

   With these conditions in mind were the dimentions in the model gradually reduced over several simulations, while the element size was kept constant. Then the element size was reduced in the new and smaller model, until it was less than one sixth of the smallest wavelength. The sequence of simulations with the applied changes is listed in table 4.3, along with the resulting number of elements and degrees of freedom. It should be noted that the first of these simulations is very similar to the simulation is section 4.1.

S	w [μm]	t_{load} [μm]	m1,max [μm]	m1,min [μm]	m2,max [μm]	m2,min [μm]	El	DOF
1	2500	2000	20	0.04	40	0.08	21018	56282
2	1000	1000	20	0.04	40	0.08	5039	15861
3	500	500	20	0.04	40	0.08	1734	6416
4	200	200	20	0.04	40	0.08	485	2213
5	100	100	20	0.04	40	0.08	222	1120
6	50	50	20	0.04	40	0.08	161	879
7	50	50	10	0.02	20	0.04	382	2152
8	50	50	5	0.01	10	0.02	1317	7397
9	50	50	2	0.005	5	0.01	7405	41989
10	50	50	5	0.01	5	0.01	1638	8060

Table 4.3: Parameters that are varied in the simulations and their values. S = simulation number, w = width of model, $t_{load} = t_{PML}$ = thickness of load layer or PML, m1,max & m1,min = maximum and minimum element sizes for mesh in domain 1 and 2, m2,max & m2,min = maximum and minimum element sizes for mesh in domain 3 and 4, El = number of elements, DOF = degrees of freedom.

4.2.2   Results and discussion

The results from each of the simulations listed in table 4.3 are compared with those from Xtrans in order to obtain four values representing how much each simulation differ from the 1D-model. The comparison is performed by taking the value from COMSOL for one of the four variables (real admittance, imaginary admittance, magnitude of Htt or phase angle of Htt) at a given frequency, and calculate the absolute difference between this and the value of the same variable at the same frequency in Xtrans. These absolute differences/errors are then summed up and divided by the number of frequencies resulting in a mean absolute difference, which is mathematically described in eq 4.1.

$$MAE_v = \frac{1}{N} \sum_{i=1}^{N} \mid c_{v,i} - x_{v,i} \mid \tag{4.1}$$

Where MAE_v is mean absolute error for variable v. While c_v and x_v are the corresponding results from COMSOL and Xtrans respectively. Furthermore is N the number of frequencies the model was solved for in COMSOL, with i representing a certain frequency. For example would $c_{Yreal,N}$ be the obtained real admittance from COMSOL when the model was solved for a frequency of 20MHz. The MAEs for each of the simulations are listed is table 4.4. The real

S	MAE_{Yreal} [S/m^2]	MAE_{Yimag} [S/m^2]	MAE_{Httabs} [μm/(s*V)]	$MAE_{Httangle}$ [degrees/1000]
1	2.383	1.817	22.36	258.3
2	2.372	1.856	24.34	310.6
3	2.347	1.767	22.30	279.0
4	3.362	2.900	34.76	274.2
5	6.364	5.972	62.87	333.7
6	9.404	8.902	90.06	403.8
7	9.386	8.814	88.77	395.6
8	2.313	1.689	21.27	222.8
9	2.161	1.557	10.98	206.4
10	2.161	1.558	10.97	206.4

Table 4.4: Mean average errors for the simulations listed i 4.3.

and imaginary admittances in the simulations are on the scale of kS/m^2, while the magnitude and phase angle of Htt is in the order of cm/(s*V) and hundred degrees, repectively. As a consequence are the MAEs very small, indicating average errors on the scale of one thousandth of the measured values. The error is however, more prominent at local maxima and minima, as can be

seen in the plot of real admittance in figure 4.4. A comparison of simulations
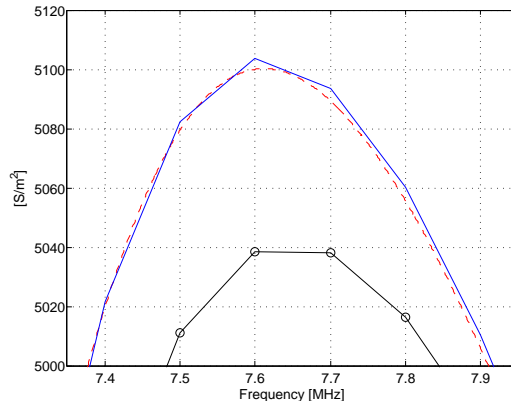

Figure 4.4: The real admittance, plotted for a small section of the simulated frequencies and a selection of the simulations listed in table 4.3. Solid blue line is simulation 10, solid black line with circle-markers is simulation 6 and dashed red line is from Xtrans.

1 and 10 shows that there is little difference in the results obtained from the respective models. However, the former has seven times the DOFs than the latter, and almost thirteen times the number of elements. Indeed the smaller model is only marginally more accurate, but much easier to solve. The reason for this is the small element size which gives a resolution of 11.5 elements per wavelength in the epoxy for a shear wave with a frequency of 20MHz. The improvement can also be seen when comparing the form of the pressure wave in water, as seen in figure 4.5. A further reduction of the element size proved to have little or no effect effect on the result, as seen when comparing the MAEs from simulations 9 and 10.

4.3 Plane water-loaded PZT-5H plate with epoxy matching layer and air backing

4.3.1 Modeling

The natural succession in the development of the model was at this point to eliminate the assumption of a incompressible backing layer and instead include a more realistic one. The backing should, in the same way as the load, be acting as a infinitely thick layer to avoid reflecting waves and thus be similar to the model in Xtrans. This could, again in the same way as in the load, be achieved with a PML. The existing model was extended by

33

(a) Maximum element size: 40μm.   (b) Maximum element size: 5μm, upper part is the PML absorbing the wave.
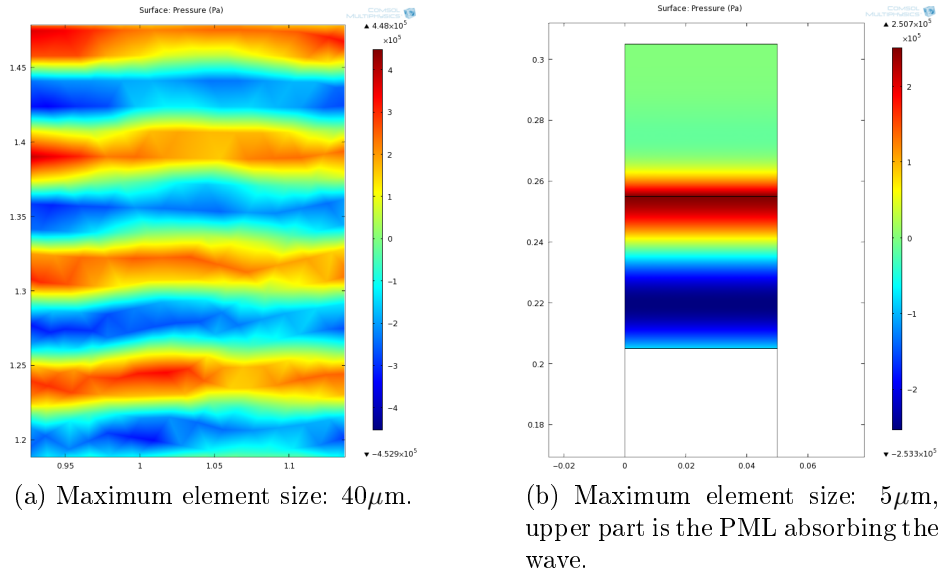
Figure 4.5: Surface plot of pressure variation in water, cause by the propagation of a 20MHz longitudinal wave.

adding two domains, as seen in figure 4.6. With the domains in order from 1 to 6 being: PML for backing, backing layer, piezoelectric layer, matching layer, load layer, PML for load. The backing layer and its PML have the same thickness as the load layer, i.e. 50μm. Domains 1 and 2 were set to be solved by the pressure acoustics interface in order to simulate air backing, and consequently the material in said domains was set to be air. All boundary conditions for domains 3-6 were the same as in section 4.2, exept from the roller condition, which was replaced by a boundary load condition in order to couple to the new acoustic domains. In domain 2 was a normal acceleration condition applied the upper boundary to couple with the piezoelectric domains, and domain 1 was set to be, as previously mentioned, a PML.

The model was meshed with the same conditions to element size as in simulation 10 in section 4.2, which will from here on be refered to as the standard meshing. This resulted in a total of 2172 elements and 9189 degrees of freedom. Afterward was the model solved for the standard frequency range.

4.3.2 Results and discussion

Admittance and Htt was obtained as described in section 3.2.7 and plotted as seen in figure 4.7. These plots prove that the model still behaves very much like the one-dimentional model in Xtrans. Despite the fact that the
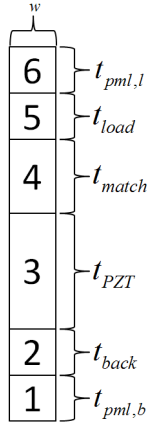
34

Figure 4.6: Geometry of the model, w = width of model, t_{PZT} = thickness of piezoelectric layer, t_{match} = thickness of matching layer, $t_{load} = t_{back} = t_{PML,l} = t_{PML,b}$ = thickness of load layer, backing layer, and their PMLs, respectively.
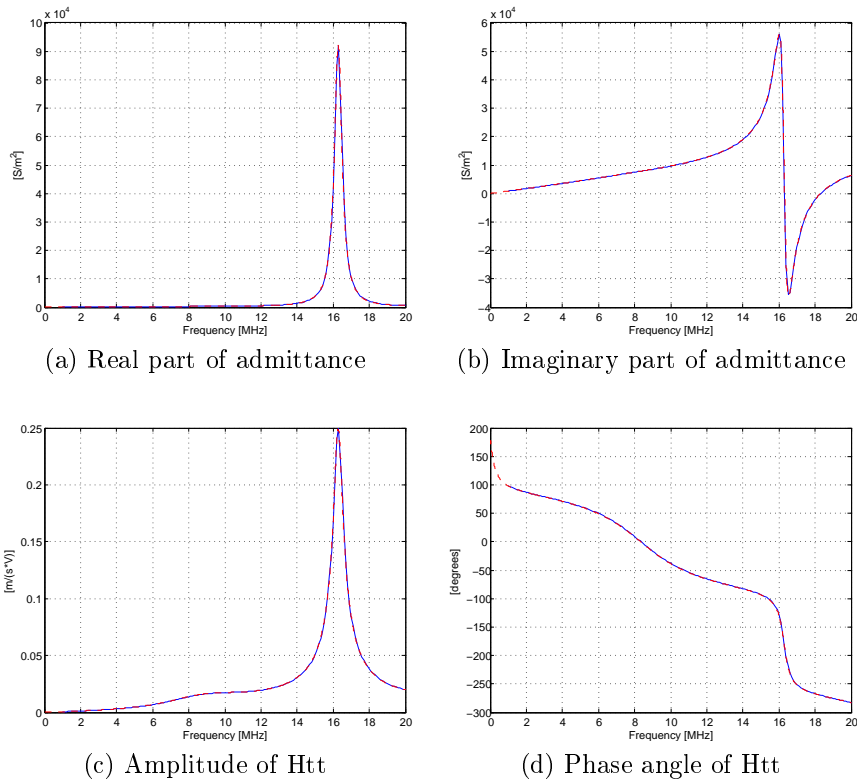

(a) Real part of admittance

(b) Imaginary part of admittance

(c) Amplitude of Htt

(d) Phase angle of Htt

Figure 4.7: Admittance and Htt found in COMSOL (blue line) and Xtrans (red, dashed line) for the model with air backing.

wavelength of a 20 MHz pressure wave in air is 17.16μm, resulting in a resolution of less than 3.5 elements per wavelength. This can be explained by the low acoustic impedance of air compared to PZT-5H, resulting in almost total wave reflection at the boundary between domain 2 and 3[23].

4.4 Plane water-loaded PZT-5H plate with epoxy matching layer and polystyren backing

4.4.1 Modeling

In this model was the air backing in the previous section replaced with that of polystyren. This is a solid, so domains 1 and 2 were changed to be governed by the piezoelectric interface, and symmetry conditions were set on the left and right boundaries of these domains. Consequently was the coupling between domains 2 and 3 removed, and a roller condition was applied to the lower boundary of domain 1. Furthermore was this domain set to be a PML, and its thickness was increased to 100μm to ensure that any wave would be sufficiently absorbed. The matching wavelength of this PML was set to be inversely proportional to the frequency, as described in section 3.2.5. Finally was the model solved with the standard element size for the standard frequency range.

4.4.2 Results and discussion

The resulting values for the admittance and Htt are, as seen in figure 4.8, indentical to the results from Xtrans. Thus proving that the PML successfully absorbs the waves. A consecutive test followed where the thickness of the piezoelectric PML was halved, this however gave some deviations in the phase angle at the lowest frequencies. As a result was the thickness kept at 100μm to keep a margin of safety.

4.5 Inclusion of mechanical loss

4.5.1 Modeling

As stated in section 2.3 are all materials lossy, and it would therefore be highly advantageous to include losses into the model described in the previous section. The type of loss included was however limited to mechanical attenuation, for the sake of simplicity. Furthermore was the loss assumed to
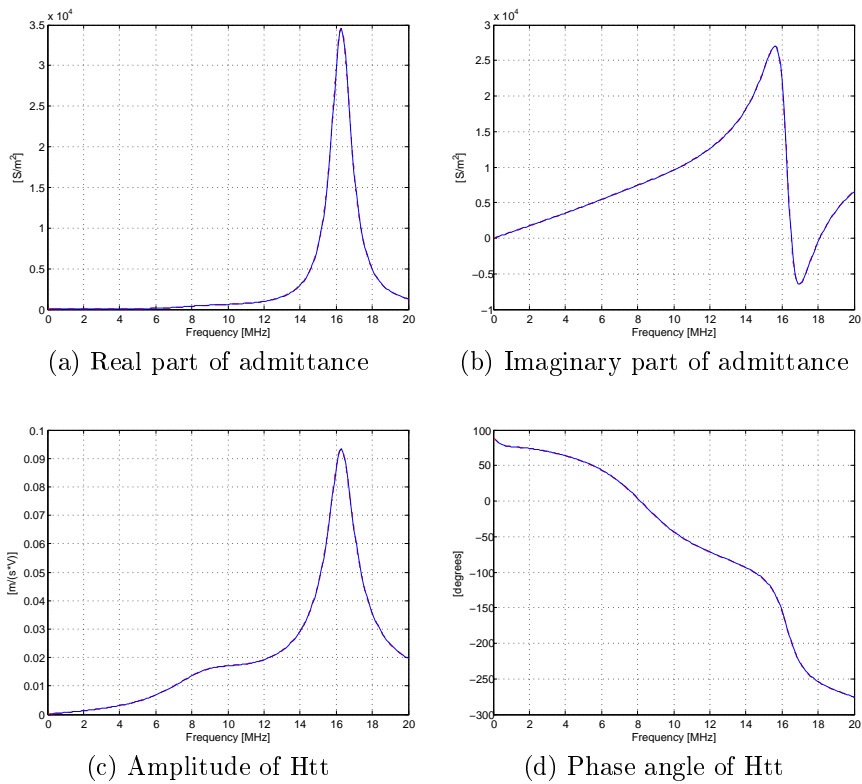
(a) Real part of admittance

(b) Imaginary part of admittance

(c) Amplitude of Htt

(d) Phase angle of Htt

Figure 4.8: Admittance and Htt found in COMSOL (blue line) and Xtrans (red, dashed line) for the model with polystyren backing.

37

be isotropic, and set to 5dB/cm/MHz for all the materials. With the relations in appendix B could then the loss factors, attenuation coefficient and Q-factors in table 4.5 be calculated. In the acoustics interface was the at-

| Material	Isotropic loss factor [unitless]	Attenuation coefficient [dB/λ]	Q-factor [unitless]
Water	-	0.74050	36.8501
Epoxy	49.1329e-3	-	20.3529
PZT-5H, initial	84.6339e-3	-	11.8156
Polystyren	43.8013e-3	-	22.8304

Table 4.5: The parameters for inclusion of loss in COMSOL and Xtrans.

tenuation of water included by changing the fluid model from linear elastic to linear elastic with attenuation, and adding the attenuation coeffiecient from table 4.5. While the loss factors were added in the material parameters as isotropic loss factors for the stiffness matrix, c^E, and included into the model through the damping and loss condition. It must here be repeated that the PMLs define their own material model, and losses must be included in these in the same way as in the regular domains. Failure to do so will result in an abrupt change in material parameters at the boundary of the PML, and negate the reflectionless quality of the boundary. Finally were the Q-factors set in Xtrans, thus replacing the previous values of 10000 that were set to represent no loss.

The simulation was then performed with loss applied to all domains. Followed by one with loss in all domains exept the piezoelectric layer (domain 3), and two with loss in only domain 3 where the loss factor was first set at the initial isotropic value, then adjusted to be anisotropic.

4.5.2 Results and discussion

The initial simulation indicates, as seen in 4.9 (a) to (d), that the damping in at least one of the layers in COMSOL is lower than in the corresponding layers in Xtrans. An assumption was made that the layer in question was the piezoelectric one, as it is the most complex layer. The second simulation, 4.9 (e) to (h), confirm this, as the results from COMSOL are essentially the same as in Xtrans. Some small deviation can however be seen in the phase angle for the absolutely lowest frequencies. This look similar to the deviations seen when the thickness of the piezoelectric PML was reduced in the previous section, and it is therefore concluded that the PML has some problems in absorbing the longest wavelengths when loss is implemented. A
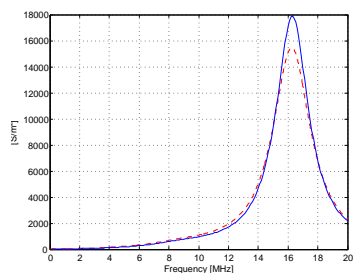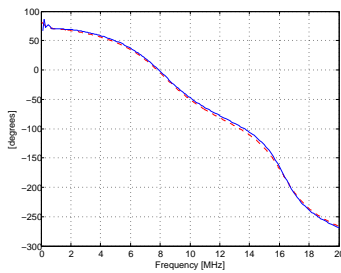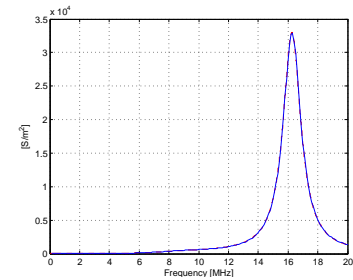
(a) Real part of admittance
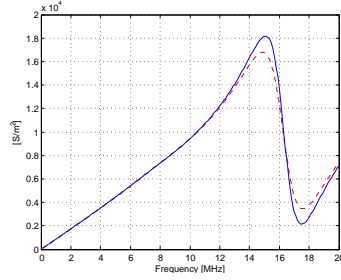
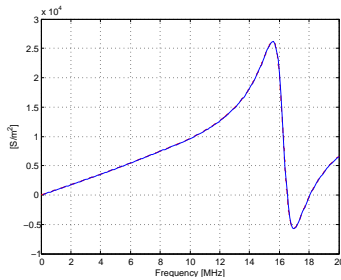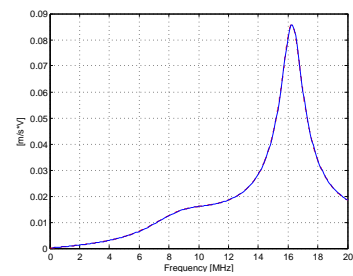(b) Imaginary part of admittance
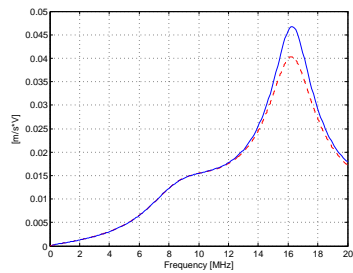
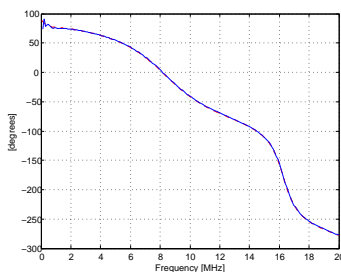(c) Amplitude of Htt

(d) Phase angle of Htt

(e) Real part of admittance

(f) Imaginary part of admittance

(g) Amplitude of Htt

(h) Phase angle of Htt

Figure 4.9: Admittance and Htt found in COMSOL (blue line) and Xtrans (red, dashed line) for loss in all domains (a-d), and for loss in all domains except the piezoelectric (e-h).

39

simple solution to this is to increase the thickness of the piezoelectric PML, but that will also give a longer computation time for the model.

It was realized that the inital calculation of the loss factor for the piezoelectric layer was erroneous. This is because the relations in appendix B yield the loss factor for the stiffness matrix under constant electric displacement field, $\boldsymbol{c}^D$, while the loss factor in COMSOL is for the stiffness matrix under constant electric field, $\boldsymbol{c}^E$. The relation between these stiffness matrices can be derived from eqs 2.22 to be:

$$\boldsymbol{c}^E = \boldsymbol{c}^D - \boldsymbol{e}^t \boldsymbol{h} \tag{4.2}$$

For the epoxy and polystyren are all the piezoelectric constant set at zero, and consequently will the loss factors be the same in both stiffness matrices. This is however not the case for the piezoelectric, and the resulting loss factor for $\boldsymbol{c}^E$ will be anisotropic. This was calculated and inplemented in the model, which resulted in a plot of the amplitude of Htt as seen in figure 4.10. Here

(a) Isotropic loss factor (b) Anisotropic loss factor
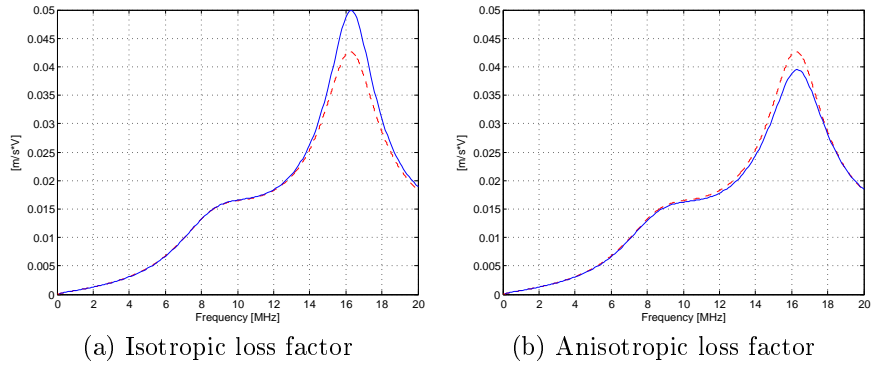
Figure 4.10: Amplitude of Htt for isotropic erroneous loss factor and anisotropic loss factor, COMSOL (blue line) and Xtrans (red, dashed line).

it can be seen that the anisotropic loss factor also yields an erroneous result. Due to time limitation was the implementation of loss thus abandoned, and is not included in later models.

4.6   Circular disc

4.6.1   Modeling

Up until this point had the model, as previously mentioned, been designed to emulated a plate of infinite lateral dimentions, and thus been directly comparable to Xtrans. This would however not be the situation for an actual

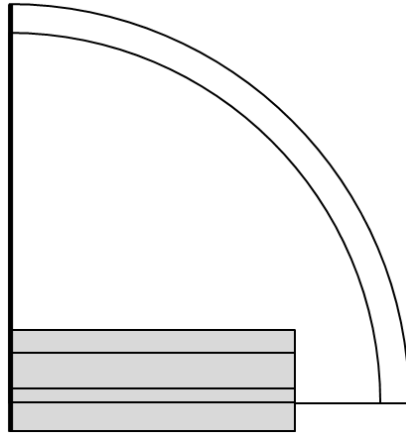Figure 4.11: Geometry of 2D-axisymmetrical model of a circular disc. Grey areas are the piezoelectric domains, while the white are the acoustic domains. The thick line to the left is the axis of symmetry.

transducer, hence should the lateral dimentions of the model be limited. The new model was designed in a two-dimentional axisymmetrical system, consequently it would emulate a circular disc. Furthermore were the thickness and material of the matching, piezo and backing layer and the piezoelectric PML set to be the same as in the two-dimentional model. While the width of these layers, which in the axisymmetrical system becomes the radius of the disc, was set as 1mm. The load was, as before, water. It was however redesigned to the shape of a quadrant with a radius of 1.3mm, hence it would have the form of a hemisphere when the model is rotated around its axis of symmetry. Moreover was the acoustic PML designed as a 0.1mm thick layer covering the load, and set to absorb wave in the radial direction. The entire geometry is depicted in figure 4.11 where grey areas indicate piezoelectric domains, while white domains are acoustic. Unlike the two-dimentional model is there no need for a second coordinate system, as axes in the axisymmetrical system are R and Z. Hence the piezoelectric is poled in the Z-direction. All conditions in the model was otherwise the same as in the two-dimentional model, exept from the coupling between the piezoelectric and acoustic interfaces, which was extended to also include the right side of the matching, piezo and backing layer. And of course the symmetry condition was replaced by the axial symmetry.

The mesh of this model was the same as previously for the piezoelectric layers, but the maximum and minimum sizes of the elements were doubled in the acoustic domains. This significantly reduced the complexity of the model, while the resolution in the domain was reduced to a minimum of 7.4

elements per wavelenght, which is acceptable. The model was still solved for the standard frequency range.

4.6.2   Results and discussion

The admittance and Htt of the transducer model was obtained through the use of line integral as mentioned in section 3.2.7, and compared with results from Xtrans as seen in figure 4.12. These plots clearly show, as expected, that

(a) Real part of admittance

(b) Imaginary part of admittance

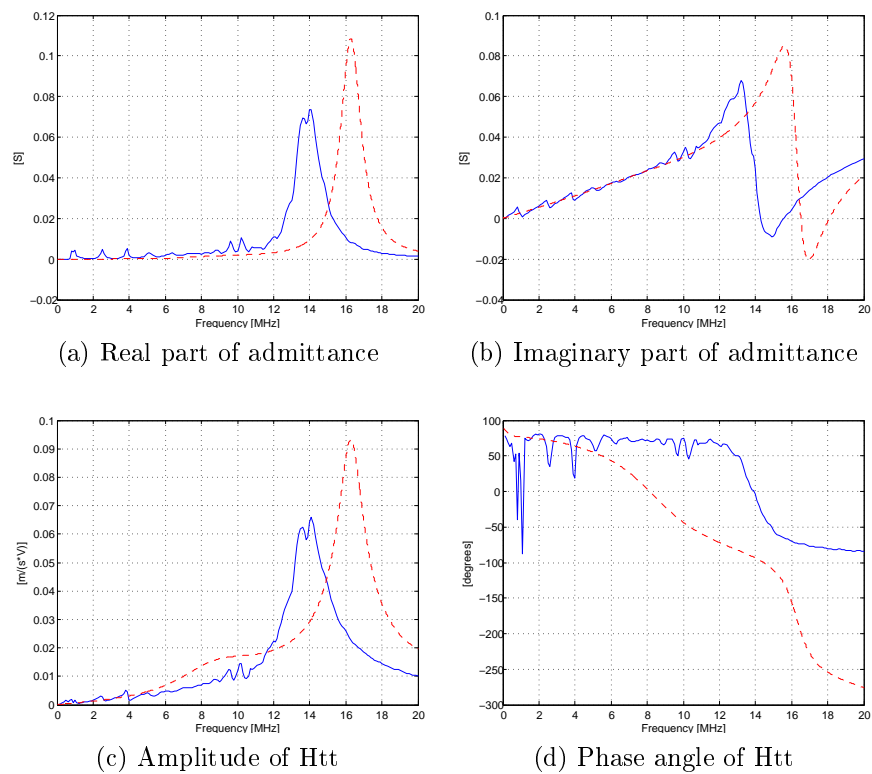(c) Amplitude of Htt

(d) Phase angle of Htt

Figure 4.12: Admittance and Htt found in COMSOL (blue line) and Xtrans (red, dashed line).

the model in COMSOL is no longer in accordance with the one-dimentional model of Xtrans. The small peaks at lower frequencies indicate that lateral modes are present. However the thickness mode is still clearly dominant, though the resonant frequency is lower than in the one-dimentional. An increase in the ratio between the radius and the thickness of the piezoelectric layer should give the transducer a behaviour closer to the one-dimentional case, and as the ratio increases towards infinity will this model approximate the behaviour of the model in section 4.4.

4.7 Circular disc with spherical coordinate system

4.7.1 Modeling

The final transducer model in this thesis will require a way of simulating a piezoelectric material that is poled in the radial direction in a spherical coordinate system in a model with a cylindrical coordinate system. The derivation of such a coordinate system is given in appendix C, however it would be wise to test the coordinate system before the final model is designed. This was done by applying the new coordinate system to the model in the previous section and setting $r_0 = 0$ and $z_0 = -1000m$, but keeping the model otherwise unaltered. As the model is placed near origo of the global coordinate system should the two systems be very close to identical within the model, and the results of this simulation should be very similar to those obtained in the previous section.

4.7.2 Results and discussion

The results from this simulation is plotted along with those from the previous simulation in figure 4.13. It can here be seen that the two results are identical, thus indicating that the spherical coordinate system is correctly implemented.

4.8 Thick film PZT on a spherical cap

4.8.1 Modeling

The final model was a further development of the 2D-axisymmetrical model in sections 4.6 and 4.7. But there were some changes in the geometry, as seen in figure 4.14. The gray areas are, as before, the domains governed by the piezoelectric devices interface, while the white domains are governed by the pressure acoustics interface. In addition is the piezoelectric layer marked with a darker shade of grey, and its position shows that this transducer model has no matching layer. The various domains in this model are, listing from top to bottom along the axis of symmetry, acoustic PML, load, piezoelectric layer, backing layer, piezoelectric PML. The load is in the shape of a quadrant with a radius of 1.3mm, while the acoustic PML covers the the arc of the quadrant with a constant layer thickness of 0.15mm. This increase in in thickness of the PML was to improve the absorpsion of waves that does not perfectly coincide with the direction of absorpsion, which was set to be in the radial

(a) Real part of admittance　　(b) Imaginary part of admittance
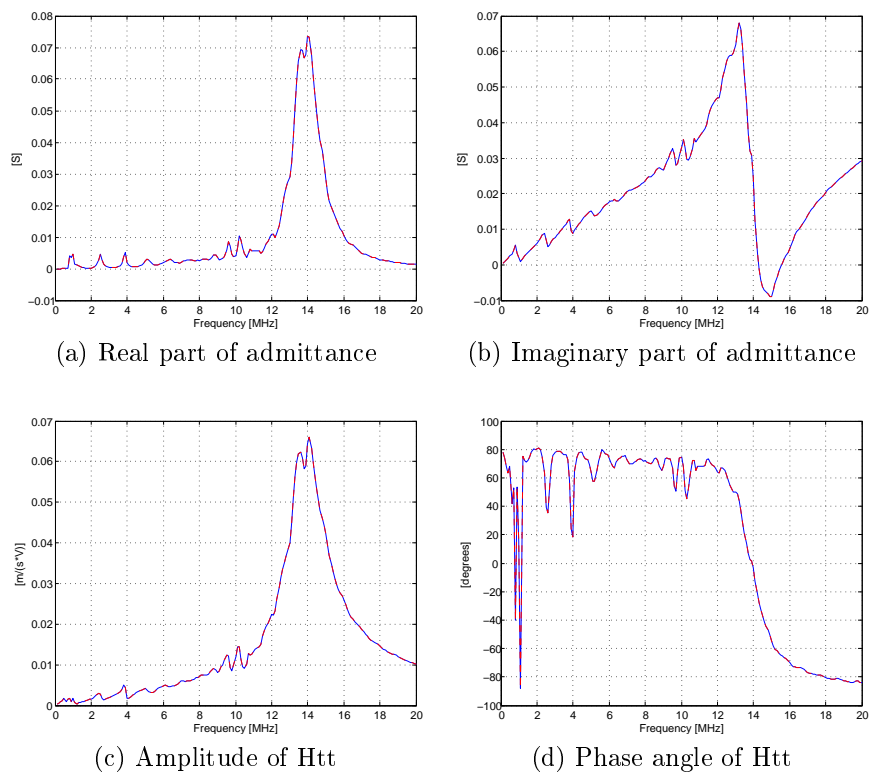
(c) Amplitude of Htt　　(d) Phase angle of Htt

Figure 4.13: Admittance and Htt found in with spherical coordinate system (blue line) and with global coordinate system (red, dashed line).
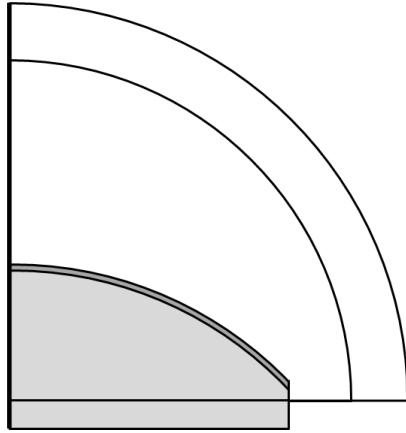
Figure 4.14: Geometry of the thick film transducer model, grey domains are governed by the piezoelectric interface, while white domains are governed by the acoustic interface. The thick line to the right is the axis of symmetry.

direction. The backing layer is in the shape of half a circle segment with a radius of 1.7mm and a chord of 2.4mm, thus giving the width of of the backing layer domain in the model as 1.2mm. Moreover is the piezoelectric layer set to cover the backing layer with a constant thickness of 25 μm in the radial direction, thus representing a thick film deposited on the surface of the backing layer. It can be seen in the figure that the backing layer is somewhat extended in the z-direction. This extension if of the same thickness as the piezoelectric layer in the z-direction at this position, approximately 35μm. Below the backing layer is the piezoelectric PML with a thickness of 0.1mm and the same width as the backing, 1.2mm. The boundary conditions are much the same as before, with a electric potential of 100V on the lower and ground on the upper boundary of the piezoelectric layer. The coupling between the acustic and piezoelectric interfaces is set on all boundaries shared by a grey and white domain. And a roller condition is, as usual, applied to the lower boundary of the piezoelectric PML. Furthermore was the piezoelectric model oriented after the spherical coordinate system in appendix C.

The material of the piezoelectric layer was set as a PZT/PGO piezo-electric thick film [10] [19]. The available material data on this thick film, although sufficent for a 1D model, was not complete for a full material speci-fication as required in COMSOL. Consequently a series of assumption had to be made of the thick films behaviour in the directions perpendicular to the poling direction. The first assumption was that the thick film still exhibits the same material symmetry as bulk PZT, thus reducing the number of unk-nown variables. Furthermore is it stated in the data sheet of the thick film

45

that it is based on Pz26 from Ferroperm, for which a full material description can be obtained [8]. A minimum of assumptions were made, based on the properties of Pz26, and all other necessary values were derived from these, yielding the thick film material listed in appendix A.

The backing material was a porous substrate of unpoled PZT [19], also without complete material data available. However, in this case only two assumptions had to be made. Firstly, that being unpoled, the material would have an isotropic behaviour. And secondly, that the Poisson's ratio of the material was 0.3 [16]. The porous PZT was also set as the material for the piezoelectric PML, while water was set as material in the load and acoustic PML.

The model was meshed with the same element size conditions as in section 4.6, and solved for the standard frequency range. Afterwards was a second simulation carried out, where an additional material model was included and applied to the backing layer. This was done to see if anything would change if the backing layer no longer was oriented after the spherical coordinate system.

4.8.2   Results and discussion

The results as seen in figure 4.15 are not very promising. The imaginary part of the admittance is approximately 50 times higher than the real part and directly proportional to the frequency. This is a property of capacitors, indicating that there is little piezoelectric coupling in the material. However, the plots of Htt show that there is a piezoelectric effect present. Furthermore can a negative real admittance, which is physically impossible, be seen at low frequency. This can however be an effect of the approximative nature of the finite element method, considering the low value of the admittance. Nevertheless, there is clearly something wrong in the model. A second simulations was, as mentioned, carried out with previously used materials. The results from this is plotted along with the results of the initial simulation in figure 4.16. It can be observed that the results of the second simulation is a lot less chaotic than those of the initial, and it should especially be noted that Htt is fairly stable for a large portion of the frequency range. Nevertheless, the admittance is still almost completely imaginary, and there is still a negative real admittance at low frequencies. But, the most important observation in a comparison of these two simulations is that they yield different results. In fact, a isotropic material should have exactly the same behaviour in the two simulations, assuming that the spherical coordinate system was implemented correctly. Unfortunately was further work hindered by the time limitation of the project, and the final model was left incomplete.
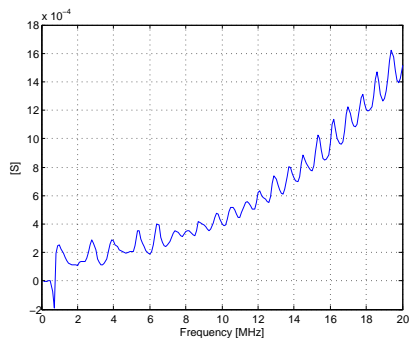
(a) Real part of admittance
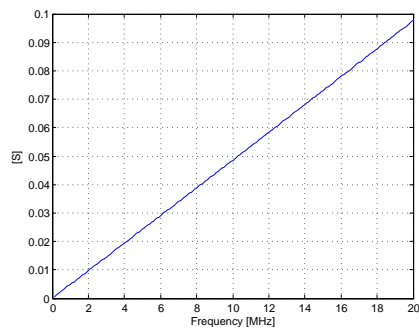
(b) Imaginary part of admittance
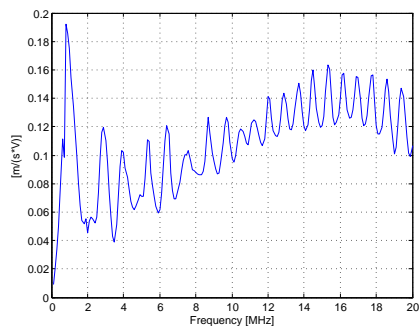
(c) Amplitude of Htt

(d) Phase angle of Htt

Figure 4.15: Admittance and Htt found in the initial simulation (blue line) of a cap transducer.
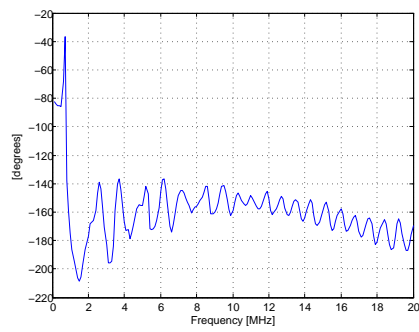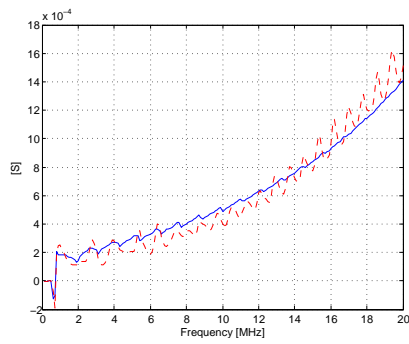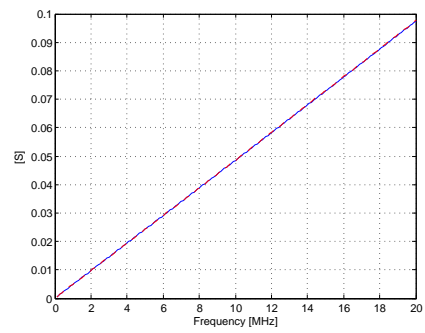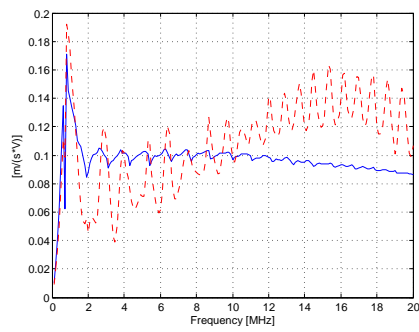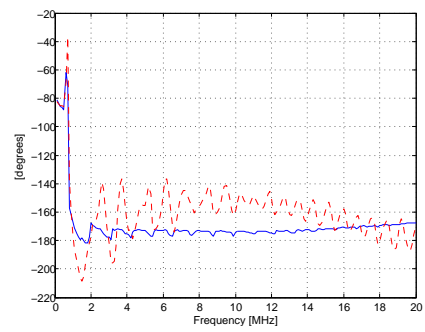
47

(a) Real part of admittance

(b) Imaginary part of admittance

(c) Amplitude of Htt

(d) Phase angle of Htt

Figure 4.16: Admittance and Htt found in second simulation (blue line), and in initial simulation (red, dashed line).

Chapter 5

Conclusion and further work

The use of COMSOL Multiphysics makes it easier for a person to start with finite element modeling, but the learning curve is still quite steep. It is important have a good understanding of the physics in question, and a basic knowledge of finite element analysis, to be able to effectively utilize such a comprehensive simulation program as COMSOL.

Finite element modeling has proven to be a useful way of simulating piezoelectric ultrasonic transducers. The method is versatile as it can be used to emulate both one-dimentional models and more realistic three-dimentional transducer models. However, the suggested minimal requirement of 6 elements per wavelength would cause the solution of a complete three-dimentional model to become practically unattainable. Thankfully can many models be significantly reduced in size, and sometimes also in dimentions, when mirror and rotational symmetry is taken into consideration. Nevertheless, solving a two-dimentional axisymmetrical model of an entire transducer is still very time consuming, but not insurmountable.

Furthermore was mechanical loss successfully implemented in the acoustic interface, and in nonpiezoelectric materials in the piezoelectric devices interface. Attempts were also made at including mechanical loss in the piezoelectric material, but the correct method for inclusion of such a loss was not reached. Further work should be done to correct this, and also to implement dielectric and piezoelectric loss in the model.

The implementation of a piezoelectric material that was not poled in a constant direction relative to the global coordinate system proved to be a challenge in this thesis, and resulted in an flawed model of the thick film transducer. Limitations in time did not allow for any further work on this model, but it should definitely be an object of further work.

Finally, the importance of correct material data must be emphasized, as a model can never be more correct than the conditions it is based on. For

this reason should further work be done in the characterization of the PZT thick film and porous substrate that was used in the final simulation.

Bibliography

[1] B. A. Auld. Wave propagation and resonance in piezoelectric materials. *The Journal of the Acoustical Society of America*, 70(6):1577–1585, 1981.

[2] R. S. R. B. Jaffe and S. Marzullo. Properties of piezoelectric ceramics in the solid-solution series lead titanate-lead zirconate-lead oxide: Tin oxide and lead titanate-lead hafnate. *Journal of Research of the National Bureau of Standards*, 55, 1955.

[3] J.-P. Berenger. A perfectly matched layer for the absorption of electromagnetic waves. *J. Comput. Phys.*, 114:185–200, October 1994.

[4] R. S. C. Cobbold. *Foundations of biomedical ultrasound.* Oxford University Press, 2006.

[5] COMSOL AB. *COMSOL Multiphysics documentation.*

[6] COMSOL AB. *Piezoacoustic Transducer*, 2010.

[7] I. Edler and H. Hertz. The use of ultrasonic reflectoscope for the continuous recording of the movements of heart walls. *The Royal Physiographic Siciety at Lund*, 1954.

[8] Ferroperm. Material data. `www.ferroperm-piezo.com`.

[9] A. Hrenikoff. Solution of problems in elasticity by the framework method. *Journal of Applied Mechanics*, 8, 1941.

[10] InSensor. *TF2100, PZT thick film based on Ferroperm Pz26.*

[11] A. D. P. Jerry H. Ginsberg and X. F. Wu. A variational principle for sound radiation from vibrating bodies. Technical report, School of Mechanical Engineering, Georgia Institute of Technology, 1986.

[12] S. G. Johnson. Notes on perfectly matched layers (pmls). Technical report, MIT, 2010.

[13] R. Lerch. Simulation of piezoelectric devices by two- and three-dimensional finite elements. *IEEE transactions on Ultrasonics, Ferroelectric and Frequency Control*, 37, 1990.

[14] Y. Liu. Introduction to the finite element method. Lecture Notes.

[15] W. Mason. Electromechanical transducers and wave filters. *Van Nostrand, Princeton, N.J.*, 1948.

[16] m. p. d. Matweb. `www.matweb.com`.

[17] e. a. Najib N. Abbouda. Finite element modeling for ultrasonic transducers. *Proc. SPIE Int. Symp. Medical Imaging*, 1998.

[18] e. a. O. C. Zienkiewicz. *The finite element method: its basis and fundamentals*. Elsevier Butterworth-Heinemann, 5 edition, 2005.

[19] e. a. Pierre Marechal. High-frequency transducers based on integrated piezoelectric thick films for medical imaging. *ieee transactions on ultrasonics, ferroelectrics, and frequency control*, 53(8), 2006.

[20] Pinin. Released into the public domain, Wikimedia Commons.

[21] A. J. Rogers, E. D. Light, D. von Allmen, and S. W. Smith. Real-time 3d ultrasound guidance of autonomous surgical robot for shrapnel detection and breast biopsy. *Medical Imaging 2009: Ultrasonic Imaging and Signal Processing*, 7265(1):72650O, 2009.

[22] K. Shung and G. Thieme. *Ultrasonic scattering in biological tissues*. CRC Press, 1993.

[23] T. L. Szabo. *Diagnostic Ultrasound Imaging: Inside Out*. Elsevier Academic Press, 2004.

[24] K. Tanaka and T. Wagai. Ultrasonic diagnosis of brain disease in japan. In *Ultrasound as a Diagnostic and Surgical Tool*, 1964.

[25] B. T.F.Johansen. Versatile analysis of multilayer piezoelectric transducers using an admittance matrix approach. *28th Scandinavian Symposium on Physical Acoustics*, 2005.

[26] K. Uchino and S. Hirose. Loss mechanisms in piezoelectrics: how to measure different losses separately. *Ultrasonics, Ferroelectrics and Frequency Control, IEEE Transactions on*, 48(1):307 –321, Jan. 2001.

[27] J. J. Wild and J. M. Reid. Application of echo-ranging techniques to the determination of structure of biological tissues. *Science*, 115, 1952.

[28] J. Yang. *An Introduction to the Theory of Piezoelectricity*. Springer Science, 2005.

Appendix A

Material data

Epoxy

Isotropic material, hence not piezoelectric.

Density	$\rho = 1210\frac{kg}{m^3}$
Stiffness matrix	$c_{11}^E = 8.7e9Pa$
	$c_{12}^E = 5.5e9Pa$
	$c_{44}^E = 1.6e9Pa$
Relative permittivity	$\epsilon_r^S = 10$
Speed of pressure wave	$v_l = 2681.4329\frac{m}{s}$
Acoustic impedance	$Z = 3.244533MRayl$

Polystyren

Isotropic material, hence not piezoelectric.

Density	$\rho = 1050\frac{kg}{m^3}$
Stiffness matrix	$c_{11}^E = 6e9Pa$
	$c_{12}^E = 5.3e9Pa$
	$c_{44}^E = 2.735e9Pa$
Relative permittivity	$\epsilon_r^S = 10$
Speed of pressure wave	$v_l = 2390.4572\frac{m}{s}$
Acoustic impedance	$Z = 2.509980MRayl$

PZT-5H

Transversely isotropic, piezoelectric.

Density	$\rho = 7500\frac{kg}{m^3}$
Stiffness matrix	$c_{11}^E = 1.27205e11Pa$
	$c_{12}^E = 8.02122e10Pa$
	$c_{13}^E = 8.46702e10Pa$
	$c_{33}^E = 1.17436e11Pa$
	$c_{44}^E = 1.6e9Pa$
Coupling matrix	$e_{31} = -6.62281\frac{C}{m^2}$
	$e_{33} = 23.2403\frac{C}{m^2}$
	$e_{15} = 17.0345\frac{C}{m^2}$
Relative permittivity	$\epsilon_{r11}^S = 1704.4$
	$\epsilon_{r33}^S = 1433.6$
Speed of pressure wave	$v_l = 4618.9008\frac{m}{s}$
Acoustic impedance	$Z = 34.641756MRayl$
h-coefficient	$h_{33} = 18.3176e8\frac{V}{m}$

Thick film PZT

Available material parameters were only sufficent for a 1D model. A series of assumptions were made based on the material properties of Ferrroperms PZ26.

Density	$\rho = 5425\frac{kg}{m^3}$	
Stiffness matrix	$c_{11}^E = 5.42787e11Pa$	calculated from assumptions
	$c_{12}^E = 1.72871e11Pa$	calculated from assumptions
	$c_{13}^E = 1.44000e11Pa$	
	$c_{33}^E = 4.51816e10Pa$	
	$c_{44}^E = 1.59683e10Pa$	calculated from assumptions
Coupling matrix	$e_{31} = 0.213342\frac{C}{m^2}$	
	$e_{33} = 6.74731\frac{C}{m^2}$	
	$e_{15} = 2.05839\frac{C}{m^2}$	calculated from assumptions
Relative permittivity	$\epsilon_{r11}^S = 438$	assumed
	$\epsilon_{r33}^S = 370$	
Speed of pressure wave	$v_l = 3300\frac{m}{s}$	
Acoustic impedance	$Z = 17.9MRayl$	
h-coefficient	$h_{33} = 20.5959e8\frac{V}{m}$	

Substrate PZT

Assumed isotropic material, hence not piezoelectric. Assumed a Poisson's
ratio of 0.3 and relative permittivity equal to the other isotropic material.

Density	$\rho = 6660 \frac{kg}{m^3}$
Stiffness matrix	$c_{11}^E = 4.9636e10 Pa$
	$c_{12}^E = 2.1272e10 Pa$
	$c_{44}^E = 2.8363e10 Pa$
Relative permittivity	$\epsilon_r^S = 10$
Speed of pressure wave	$v_l = 2730 \frac{m}{s}$
Acoustic impedance	$Z = 18.2 MRayl$

Water

Density	$\rho = 999.6 \frac{kg}{m^3}$
Speed of pressure wave	$v_l = 1481 \frac{m}{s}$
Acoustic impedance	$Z = 1.480871 MRayl$

Air

Density	$\rho = 1.204 \frac{kg}{m^3}$
Speed of pressure wave	$v_l = 343.2 \frac{m}{s}$
Acoustic impedance	$Z = 0.004133 MRayl$

Appendix B

Derivation of the different representations of mechanical loss

A wave with loss can be expressed as:

$$e^{-j\frac{\omega}{c}(1-j\alpha)z} \tag{B.1}$$

Where c is the wave velocity, ω is the angular frequency and α is the attenuation factor. The wave velocity can also be written as the complex wave velocity $c*$ giving:

$$\frac{\omega}{c^*} = \frac{\omega}{c}(1 - j\alpha) \tag{B.2}$$

Which can, when assuming $j\alpha$ much smaller than 1, be written as:

$$c^* \approx c(1 + j\alpha) \tag{B.3}$$

Applying the relation between the stiffness matrix in an isotropic material and the wave velocity yields:

$$M^* = c^{*2}\rho \approx c^2(1 + 2j\alpha) \tag{B.4}$$

Where M is the P-wave modulus. A similar calculation can aslo be made for an anisotropic material. Loss factor damping in the piezoelectric devices interface in COMSOL defines a complex modulus:

$$G^* = (1 + j\eta_S)G \tag{B.5}$$

The relation between η_S and α is therefore:

$$\eta_S = 2\alpha \tag{B.6}$$

Which is also the relation between α and the loss tangent $tan\delta$.

In the pressure acoustics interface in COMSOL can the attenuation coefficient be given as dB/λ. The relation between this coefficient (α') and α is:

$$\frac{\omega}{c}\left(1 - jln(10)\frac{\alpha'}{40\pi}\right) = \frac{\omega}{c}(1 - j\alpha)$$

$$\alpha = ln(10)\frac{\alpha'}{40\pi} \tag{B.7}$$

Loss in Xtrans is implemented through a Q-factor defined as:

$$Q = \frac{1}{2\alpha} \tag{B.8}$$

In many material data sheets is the attenuation factor defined in dB/cm/MHz, the relation between this (α'') and α is:

$$10^{-\frac{\alpha''}{20}fz10^{-4}} = e^{\frac{-2\pi f}{c}\alpha z}$$

$$\alpha = ln(10)\frac{c}{4\pi10^5}\alpha'' \tag{B.9}$$

These calculations yield a set of relations that can be used to implement the same mechanical damping in COMSOL as in Xtrans.

Appendix C

Derivation of a local spherical coordinate system in a global cylindrical coordinate system

The coordinate system is defined by three vectors: x_1, x_2 and x_3. x_2 is however already correctly defined as perpendicular to the r-z plane, and will not be discussed any further. x_1 is defined as perpendicular to the outline of a circle with radius R on any position on the outline. x_3 is defined as tangential to any point on the outline of the same circle, as seen in figure C.1. Both vectors are described by two components, one in the r-direction and the other in the z-direction. In addition must both vectors always have a length of unity. The center of the circle is set at (r_0, z_0), thus can the radius be descibed as:

$$R = \sqrt{(r - r_0)^2 + (z - z_0)^2} \tag{C.1}$$

Based on these conditions can the components of x_1 and x_3 be decided, a selection of values are listed in table C.1. From the values in this table can

Rads	Position		x_1		x_3	
	r	z	r	z	r	z
0	R	0	0	-1	1	0
$\frac{\pi}{6}$	$\frac{\sqrt{3}R}{2}$	$\frac{R}{2}$	$\frac{1}{2}$	$-\frac{\sqrt{3}}{2}$	$\frac{\sqrt{3}}{2}$	$\frac{1}{2}$
$\frac{\pi}{4}$	$\frac{R}{\sqrt{2}}$	$\frac{R}{\sqrt{2}}$	$\frac{1}{\sqrt{2}}$	$-\frac{1}{\sqrt{2}}$	$\frac{1}{\sqrt{2}}$	$\frac{1}{\sqrt{2}}$
$\frac{\pi}{3}$	$\frac{R}{2}$	$\frac{\sqrt{3}R}{2}$	$\frac{\sqrt{3}}{2}$	$-\frac{1}{2}$	$\frac{1}{2}$	$\frac{\sqrt{3}}{2}$
$\frac{\pi}{2}$	0	R	1	0	0	1

Table C.1: Values of the base vectors for some angles on the circle, assuming center of circle in (0,0)
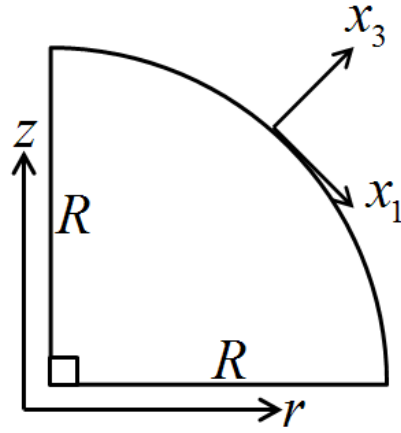
Figure C.1: Definition of global (r, z) and local (x_1, x_3) coordinate system.

x_1 and x_3 be defined as:

$$x_1 \begin{cases} r = & \frac{z-z_0}{R} \\ z = & -\frac{r-r_0}{R} \end{cases} \tag{C.2}$$

$$x_3 \begin{cases} r = & \frac{r-r_0}{R} \\ z = & \frac{z-z_0}{R} \end{cases} \tag{C.3}$$